

Time-Spread Pilot-Based Channel Estimation for Backscatter Networks

Fatemeh Rezaei*, *Member, IEEE*, Diluka Galappaththige*, *Member, IEEE*, Chintla Tellambura, *Fellow, IEEE*,
Amine Maaref, *Senior Member, IEEE*

Abstract—Current backscatter channel estimators employ an inefficient silent pilot transmission protocol, where tags alternate between silent and active states. To enhance performance, we propose a novel approach where tags remain active simultaneously throughout the entire training phase. This enables a one-shot estimation of both the direct and cascaded channels and accommodates various backscatter network configurations. We derive the conditions for optimal pilot sequences and also establish that the minimum variance unbiased (MVU) estimator attains the Cramér-Rao lower bound. Next, we propose new pilot designs to avoid pilot contamination. We then present several linear estimation methods, including least square (LS), scaled LS, and linear minimum mean square error (MMSE), to evaluate the performance of our proposed scheme. We also derive the analytical MMSE estimator using our proposed pilot designs. Furthermore, we adapt our method for cellular-based passive Internet-of-Things (IoT) networks with multiple tags and cellular users. Extensive numerical and simulation results are provided to validate the effectiveness of our approach. Notably, at least 10 dBm and 12 dBm power savings compared to the prior art are achieved when estimating the direct and cascaded channels. These findings underscore the practical benefits and superiority of our proposed approach.

Index Terms—Backscatter communication (BackCom), Pilot transmission, Channel estimation, Cramér-Rao lower bound (CRLB), Hadamard matrix, Modified Zadoff–Chu (ZC) sequences.

I. INTRODUCTION

Backscatter communication (BackCom) networks use electronic tags to reflect external radio frequency (RF) signals to transmit data. They enable passive or ambient Internet of Things (IoT) networks [1]–[6]. They comprise multiple interconnected devices that can sense, collect, and exchange information about their environment without explicit human intervention [1]–[3]. They have a wide range of applications, such as smart homes, smart cities, industrial IoT, and health-care [1]–[3]. They are under intense consideration by the third-generation (3GPP) standards for passive IoT networks [7], [8].

A typical BackCom network comprises an RF emitter, a reader, and one or multiple tags [3], where the basic configuration can be monostatic, bistatic, or ambient (Fig. 1). In monostatic BackCom (MoBC) (Fig. 1a), the reader emits the RF signal, the tag reflects it, and the reader decodes the reflected signal. In contrast, the bistatic BackCom (BiBC)

employs dedicated carrier emitters (Fig. 1b). On the other hand, ambient BackCom (AmBC) (Fig. 1c) utilizes ambient RF emitters, such as TV towers, cellular base stations (BS), Wi-Fi access points (AP), and others, to communicate with the reader. AmBC can also be a form of symbiotic radio (SR) (Fig. 1d), where the reader acts as a cooperative receiver, e.g., a smartphone, which decodes the signals of both the RF source and tags [9].

A. Channel Estimation for BackCom Networks

Channel estimation is an essential, ubiquitous task in any wireless network, which is necessary for ensuring performance, reliability, and security [10]. For example, the reader in a BackCom network needs accurate channel state information (CSI) for decoding, beamforming, signal detection, interference mitigation, security and privacy enhancements, and other tasks [10]. This need can be met by pilot-based, blind, or semi-blind techniques CSI estimators [11], [12]. Pilots, which are known symbols, improve the estimation accuracy, while blind techniques exploit received signal statistics without pilot symbols. However, their accuracy levels (in terms of mean square error (MSE)) may be low due to the absence of pilot symbols [12].

Although pilot-based techniques are widely used, they reduce spectral efficiency by limiting the amount of time available for data transmission and also increase energy consumption [13], [14]. Therefore, optimizing the trade-off between channel estimation accuracy and spectral and energy efficiencies is critical for the overall performance [13], [14].

However, the problem of BackCom channel estimation is distinct from that for conventional wireless networks and presents challenges due to the specific characteristics of the channel and the limitations of the tags. The BackCom channel is a cascaded (or dyadic) one when the signal propagates from the RF emitter to the tag and then from the tag to the reader, and a direct channel describes signal propagation from the emitter to the reader. The cascaded channel has fading characteristics that are significantly different from those of direct channels and are subject to a double path loss. These specific channel characteristics are described in [3] and references therein.

The other challenges emanate from the limitations of the tags. Firstly, tags do not generate pilot signals by themselves as they lack active RF circuits but simply reflect incident RF signals [3]. Secondly, passive tags harvest (i.e., absorb) a part of the received RF power to operate their internal circuits [3],

*F. Rezaei and D. Galappaththige contributed equally to this work.

F. Rezaei, D. Galappaththige, and C. Tellambura are with the Department of Electrical and Computer Engineering, University of Alberta, Edmonton, AB, T6G 1H9, Canada (e-mail: {rezaeidi, diluka.lg, ct4}@ualberta.ca).

A. Maaref is with Huawei Canada, 303 Terry Fox Drive, Suite 400, Ottawa, Ontario K2K 3J1 (e-mail: amine.maaref@huawei.com).

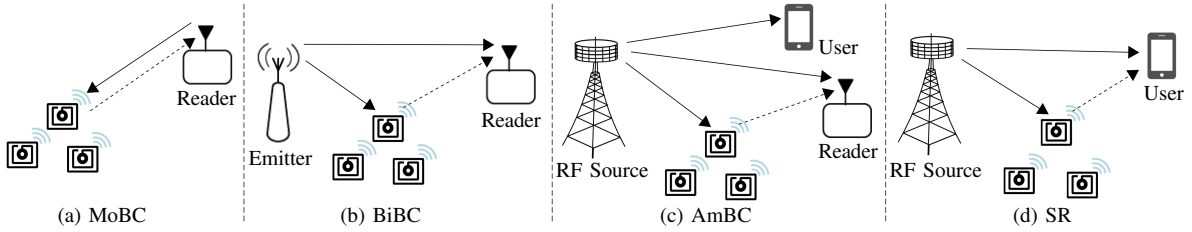


Fig. 1: Different BackCom configurations.

resulting in low reflected power levels that may be insufficient for accurate channel estimation. Furthermore, because passive tags must harvest energy, they often have low-cost, power-integrated circuits with limited processing capabilities [7], [15]. Consequently, they may not be able to transmit complex, high-power pilot sequences. These limitations indicate that traditional pilot-based channel estimation methods must be adapted carefully in this context.

Due to the vast application potential of BackCom networks, several useful channel estimation techniques have already been developed. In the following, we will briefly describe these works, emphasizing their strengths and weaknesses in order to identify gaps in the existing literature. By doing so, we set the background and context for our work.

B. Previous Contributions

We have listed the ones for AmBC [16]–[22] in Table I. As can be seen, most works focus on single-tag ($K = 1$) networks. For a network of $K \geq 1$ tags, these works rely on what may be referred to as the silent protocol. It has the essential idea of just one node transmitting pilots at a time while every other node remains silent. Thus, it divides the channel estimation interval into $K + 1$ equal slots. All the tags remain silent on the first slot except for the RF emitter. During each one of the remaining K slots, one tag reflects pilots while others remain silent. Consequently, the direct (RF source-reader) channel and the cascaded channels are estimated one by one in a round-robin manner.

However, the silent protocol (Fig. 4) has several drawbacks. Firstly, as the number of tags increases, the number of slots required also increases, resulting in longer pilot sequence lengths, and reduced energy and spectral efficiencies. Secondly, cascaded channel estimates are obtained by subtracting the direct channel estimate, resulting in error propagation and increased MSE of the estimates. To reduce the MSE, longer pilot sequences are necessary, further degrading the energy and spectral efficiencies. These critical drawbacks make the silent protocol inefficient for handling a large number of tags. We further discuss these problems in Section III-A.

Based on the silent protocol, these works employ classical and machine learning methods, including expectation maximization [16], [23], eigenvalue decomposition of the received signal’s covariance matrix [18] for blind estimation, discrete Fourier transformation (DFT) [19], deep neural networks [20], and iterative estimation [21] for pilot-based estimation. Moreover, pilot-based channel estimation has also been investigated

in large intelligent surface (LIS)-aided AmBC networks [22], building on the basic idea explored in the previous works.

In [24], the direct channel and cascaded channel are estimated simultaneously for the full-duplex ambient RF source and the legacy user. This work develops a maximum-likelihood (ML) estimator, but the extension to multiple tags is challenging. Reference [25] also leverages a deep learning approach for the joint pilot design and channel estimation in a multi-tag SR network. It first uses a deep residual network with three blocks to eliminate the noise and then exploits successive interference cancellations to estimate the direct channel and the cascaded links sequentially.

The works [26], [27] focus on MoBC channel estimation, addressing single and multiple tag scenarios. Reference [17] develops direct and cascaded channel estimators of a single tag network while accounting for carrier-frequency offsets (CFO) and in-phase/quadrature imbalance. The study [28] develops joint channel estimation, interference suppression, and data detection for an orthogonal frequency division multiplexing-based AmBC system with a single tag. The method employs the space alternating generalized expectation maximization algorithm. Reference [29] presents a two-phase uplink-training-based channel estimation approach for estimating direct and cascaded channels in a cell-free SR network with a single user and single tag. The study [30] proposes two iterative channel estimate approaches for reconfigurable intelligent surfaces (RIS)-enabled multi-user communication networks.

To summarize, the current approach of using the silent protocol is highly inefficient. Another shortcoming is the focus on the single-tag case, with a lack of solutions for multiple tags ($K > 1$), likely due to the poor scaling of the silent protocol as K increases. Furthermore, some of the proposed solutions are developed for specific configurations such as MoBC, BiBC, AmBC, and SR, which limits their generality. There have been only a few studies, such as [24], [28] and [26], [27], which have investigated setups like AmBC and MoBC, respectively.

C. Problem Statement and Contributions

To remedy these issues, we present a versatile channel estimation method for any BackCom configuration. Unlike prior solutions, our method is a one-shot estimate of all channel gains (both direct and cascaded) for an arbitrary number of tags (Fig. 2). Here, the term “one-shot estimation” refers to the simultaneous (parallel) estimation of the direct channel and all cascaded channels during pilot transmission. Unlike the silent protocol [16], [18]–[20], [26], [27], we develop the time spreading of tag pilots over the entire estimation

TABLE I: Summary of related works.

Config.	Reference	Pilot-based	Setup			Channel		Key idea
			Tags	Reader	Emitter	Fading	Path loss	
AmBC	[16]	✗ (Blind)	$K = 1$	SA	SA	Rayleigh	✗	Silent
	[17]	✓	$K = 1$	SA	SA	Rayleigh	✗	Silent
	[18]	✗ (Blind)	$K = 1$	MA	SA	Rayleigh	✗	Silent
	[19]	✓	$K = 1$	MA	SA	Rayleigh	✗	Silent
	[20]	✓	$K = 1$	MA	SA	Rayleigh	✗	Silent
	[21]	✓	$K = 1$	SA	SA	Rayleigh	✗	Silent
	[22]*	✓	LIS	SA	SA	Rayleigh	✗	Silent
	[24]†	✓	$K = 1$	MA	SA	Nakagami	✓	One-shot
	[28]	✗ (Semi-blind)	$K = 1$	SA	SA	Rayleigh	✓	Iterative
SR	[25]	✓	$K \geq 1$	SA	MA	Rayleigh	✗	Silent
MoBC	[26]	✓	$K = 1$	MA	–	Rayleigh	✓	–
	[27]	✓	$K \geq 1$	MA	–	Rician	✓	Silent
Any	This paper	✓	$K \geq 1$	MA	SA	Nakagami	✓	One-shot

SA - Single antenna MA - Multiple antenna

† The reader is a full-duplex multi-antenna AP and the emitter is the AP as well as a single antenna user.

* LIS-assisted AmBC.

interval, i.e., all tags modulate and reflect pilots simultaneously during the estimation interval. Thus, the reader sees a received signal that is a combination of pilots spread over the direct and the backscatter channels. That ensures that spatial and time resources are fully utilized for channel estimation, which enhances the estimation accuracy remarkably. We also ensure the orthogonality among tag transmissions through optimally designed pilot sequences. Hence, our method avoids pilot contamination and error propagation.

To provide practical insights, we consider both large-scale fading and small-scale fading (via the versatile Nakagami- m fading model) to model the direct channel and the cascaded channels.

The contribution of this work is summarized as follows:

- We first design an efficient pilot transmission protocol where all the tags reflect pilots during the estimation interval. We identify that the RF source acts as a hidden tag with an all-1 pilot sequence. Accordingly, we derive the necessary conditions on the tag sequences to avoid pilot contamination among the tags and the RF source.
- We reformulate the received signal at the reader into a linear equation to derive the minimum variance unbiased (MVU) estimator. The MVU estimator, which is the linear least squares (LS) estimator for the linear model, is efficient and attains the Cramér-Rao lower bound (CRLB). It thus provides a sufficient criterion to design tag sequences such that the variance of the estimation is minimized.
- We next propose and investigate novel tag pilot sequence designs, i.e., (i) rows of Hadamard matrix, (ii) modified Zadoff-Chu (ZC) sequences, and (iii) rows of DFT matrix. We find that ZC sequences do not meet the design criteria. We thus propose a method for modifying any set of orthogonal sequences for BackCom channel estimation.
- We derive classical deterministic estimators, namely LS and scaled LS, and Bayesian estimators optimal minimum mean square error (MMSE) and linear MMSE (LMMSE).

The latter two exploit the knowledge of channel statistics.

- Additionally, we generalize our method for cellular-based passive IoT networks with concurrent multiple tags and cellular users. We give extensive numerical and simulation results to demonstrate the gains of our approach compared to the silent protocol. For instance, to estimate the direct and cascaded channels, our method, compared to the silent protocol, saves 10 and 12 dBm. These are remarkable gains.

Our proposal is notably versatile, as it supports different rate inequalities between the RF source and the tags, encompassing scenarios where $R_b = R_s$ or $R_b < R_s$, where R_b and R_s are the data rates of the tag and the RF source, respectively [9]. As a result, it is applicable to different communication networks, such as cellular-based passive IoT where the rate of the user is typically higher than the rate of the tags.

D. Structure and Notations

The paper is structured as follows. In Section II, we introduce the system model and discuss the tag operations. Section III reviews prior research on the channel estimation problem, and Section III-B presents our proposed method. Section IV extends the proposed channel estimate approach to a generalized network with multiple tags and multiple users. To assess the effectiveness of our approach, we provide extensive simulation examples in Section V. Lastly, we summarize the key findings of the paper and suggest future research directions in Section VI.

Notation: \mathbf{A}^T and \mathbf{A}^H , denote transpose and Hermitian transpose, respectively. $\mathbb{E}\{\cdot\}$ denotes the statistical expectation. $\mathcal{CN}(\boldsymbol{\mu}, \mathbf{C})$ is a complex Gaussian vector with mean $\boldsymbol{\mu}$ and co-variance matrix \mathbf{C} . The operations $\text{vec}(\mathbf{X})$, \otimes , and \odot are respectively the column-wise stacked version of \mathbf{X} , Kronecker product, and Hadamard product, which refers to component-wise multiplication of two vectors of the same dimension.

Besides, $\text{diag}(\mathbf{x})$ with $\mathbf{x} \in \mathbb{C}^{1 \times N}$ returns the matrix $\mathbf{X} \in \mathbb{C}^{N \times N}$ with \mathbf{x} on the diagonal, $\mathbf{C}_{\mathbf{x}} = \text{Cov}(\mathbf{x}, \mathbf{x})$

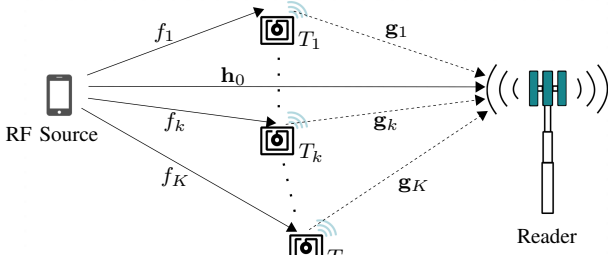


Fig. 2: AmBC system setup.

is the covariance matrix of \mathbf{x} , and $\mathbf{I}_N \in \mathbb{R}^{N \times N}$ is an identity matrix. Finally, $\mathcal{M} \triangleq \{1, \dots, M\}$, $\mathcal{K} \triangleq \{1, \dots, K\}$, $\mathcal{K}_0 \triangleq \{0, 1, \dots, K\}$, $\mathcal{K}_k \triangleq \mathcal{K}/k$, and $\mathcal{N} \triangleq \{1, \dots, N\}$.

II. SYSTEM, CHANNEL, AND SIGNAL MODELS

A. System and Channel Models

We consider an AmBC network comprising a single-antenna RF source (or user), K single-antenna passive tags (k -th tag is denoted by T_k), and a reader (or BS/AP) with M antennas (Fig. 2). The network operates on a block flat-fading channel model. During each fading block, $\mathbf{h}_0 = [h_{1,0}, \dots, h_{M,0}]^T \in \mathbb{C}^{M \times 1}$ is the direct channel response vector from the RF source to the reader. Moreover, $\mathbf{h}_k = f_k \mathbf{g}_k \in \mathbb{C}^{M \times 1}$ is the effective backscatter (cascaded) channel through T_k , which is the product of the forward-link channel from the RF source to T_k , i.e., $f_k \in \mathbb{C}$, and the backscatter channel from T_k to the reader, i.e., $\mathbf{g}_k = [g_{1,k}, \dots, g_{M,k}]^T \in \mathbb{C}^{M \times 1}$. A unified representation of all channels is given as

$$a = \alpha_a \exp(j\phi_a), \quad (1)$$

where $a \in \mathcal{A} \triangleq \{f_k, g_{m,k}, h_{m,0}\}$ for $m \in \mathcal{M}$ and $k \in \mathcal{K}$, and $\phi_a \in [-\pi, \pi]$ is the phase of a . In (1), α_a is the envelope of a , which is assumed to be Nakagami- \bar{m}_a distributed with \bar{m}_a shape and $\Omega_a = \bar{m}_a \zeta_a$ scaling parameters. Here, ζ_a accounts for the large-scale path loss and shadowing.

Remark 1. *Nakagami- m is a versatile model, which can represent a variety of propagation environments. For instance, when $m = 1$, it represents Rayleigh fading, and when $m \rightarrow \infty$, it represents the no fading scenario. Hence, our proposed channel estimation can be applied to any fading channels, e.g., Rayleigh, Rician, and others [31], [32].*

B. Tag's Data Transmission

Passive tags are electronic devices that operate their essential circuits and processing solely through energy harvesting (EH), eliminating the need for batteries. As a result, they face strict energy and power limitations. These tags modulate and reflect their data to the reader and carry out EH using two methods: time-switching and power-splitting. In the time-switching approach, the tasks are performed in separate time slots, while in the power-splitting approach, both tasks occur simultaneously, utilizing a fraction of the incident RF power [33]. Given the inability of passive tags to store energy, the power-splitting mode is generally preferred over the time-switching mode [34], [35].

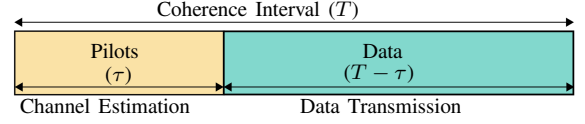


Fig. 3: Coherence interval.

We assume all tags have the same power reflection coefficient, $\alpha \in (0, 1)$. In the power-splitting mode, each tag reflects back αP_{rf} for data communication and absorbs $(1 - \alpha)P_{\text{rf}}$ for EH where P_{rf} is the incident RF power. The EH process is described in [3].

Tags employ a communication technique known as load modulation to modulate data. Load modulation involves encoding digital information into the amplitude, phase, or frequency of the backscattered signal. This is achieved by the tag dynamically switching between a predefined set of load impedances connected to its antenna. These impedance variations create mismatches, resulting in the generation of complex reflection coefficients. The collection of these reflection coefficients forms a multi-level (\tilde{M} -ary) signal constellation, enabling the tag to effectively convey data. In this paper, we consider the phases of the reflection coefficients to create the modulation alphabet. For details of such modulation methods, we refer the reader to [3], [4] and the references therein. Thus, the tag symbol $c(n)$ ($\mathbb{E}\{|c(n)|^2\} = 1$), is selected from a \tilde{M} -ary constant-envelope modulation [4].

The EH process at the tags is not within the scope of this paper. However, it is worth noting that the integration of EH into channel estimation is an intriguing topic that has not been extensively explored in existing literature. This aspect will be addressed in our future research endeavors. For readers interested in further understanding EH in BackCom networks, we recommend referring to [3] and the references cited therein.

III. CHANNEL ESTIMATION

The goal is to estimate $\mathbf{H} = [\mathbf{h}_0, \mathbf{h}_1, \dots, \mathbf{h}_K]$ using training based channel estimation method. To this end, each coherence interval comprises two phases, i.e., channel estimation and data transmission (Fig. 3). During the first phase, the RF source transmits a pilot sequence with length τ , i.e., $\sqrt{p}\mathbf{s} \in \mathbb{C}^{1 \times \tau}$, where $\mathbf{s} = [s_1, \dots, s_\tau]$ and s_i satisfies $|s_i|^2 = 1$ for $i = \{1, \dots, \tau\}$, p is the RF source transmit power, and the tags backscatter, c_k , to the reader. In the following, we consider the same data rate for the tags and the source, i.e., $R_b = R_s$. We also explore the scenario where $R_b < R_s$ in Section IV, demonstrating the versatility and generality of our proposed scheme.

The two types of BackCom channels are: i) the direct-link channel from the RF source to the reader (\mathbf{h}_0), ii) the cascaded channels, i.e., RF source-to-tag-to-reader channels ($f_k \mathbf{g}_k$, for $k \in \mathcal{K}$). These two types are estimated slightly differently.

Next, we first describe the existing pilot-based channel estimators and reiterate their limitations. We then present our approach.

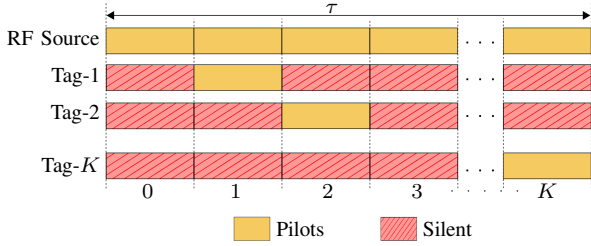


Fig. 4: Pilot transmission in the prior art.

A. Prior Art

The prior art uses what can be described as the silent protocol. It divides the channel estimation time, τ , into $K + 1$ slots, each with t pilot symbols (for equal division) [16], [18]–[20], [26], [27] (Fig. 4). In the first slot, all the tags are silent with no reflections, i.e., $c_k = 0$ for $k \in \mathcal{K}$. Thus, the reader computes the direct channel estimate $\hat{\mathbf{h}}_0$ cleanly. In each of subsequent K slots, one tag backscatters the pilot symbol $c_k = 1$ while the others do not reflect ($c_k = 0$) (Fig. 4). The reader then estimates $\mathbf{h}_0 + \sqrt{\alpha} f_k \mathbf{g}_k$, where $\alpha \in (0, 1)$ is the tag reflection coefficient, which is constant for all tags, and subtracts $\hat{\mathbf{h}}_0$. This yields the cascaded channel estimate, $\hat{\mathbf{h}}_k = \widehat{f_k \mathbf{g}_k}$ for $k \in \mathcal{K}$. We now explain this process with a specific example.

Example 1. For two tags ($K = 2$), the silent protocol needs three time slots. If the tags use pilots 0 and 1, and the RF signal is \sqrt{p} in the i -th time slot, the received signals at the reader are given as

$$\mathbf{Y}_i = \begin{cases} \sqrt{p} \mathbf{h}_0 + \mathbf{n}_0, & \text{for } i = 0, \\ \sqrt{p} (\mathbf{h}_0 + \sqrt{\alpha} f_i \mathbf{g}_i) + \mathbf{n}_i, & \text{for } i \in \{1, 2\}, \end{cases} \quad (2)$$

where \mathbf{n}_i is an additive white Gaussian noise (AWGN) term. From the received signal (2), the reader estimates \mathbf{h}_0 from \mathbf{Y}_0 . The reader then estimates $\mathbf{h}_0 + \sqrt{\alpha} f_i \mathbf{g}_i$ and subtracts $\hat{\mathbf{h}}_0$ to obtain the cascaded channel estimates.

1) *Limitations of the Prior Art:* Although the above approach may seem simple, several critical drawbacks result in poor performance. As such, it is important to identify these weaknesses in order to develop efficient and reliable alternatives. Here is a list of the limitations:

- The one-by-one estimation of the direct channel and the cascaded channels requires the estimation interval to increase with $K + 1$.
- Estimating cascaded channels through subtracting $\hat{\mathbf{h}}_0$ leads to error propagation, making the MSE of cascaded channel estimates reliant on the MSE of $\hat{\mathbf{h}}_0$. Thus, highly accurate $\hat{\mathbf{h}}_0$ estimation requires longer pilot sequences, consequently increasing pilot training overhead.
- Each channel is estimated using a few pilot symbols, i.e., \mathbf{Y}_i for $i \in \mathcal{K}_0$, Eq. (2), not all the pilots. This forces using longer pilot sequences to compensate for this design defect, increasing channel estimation overhead.
- Much of the coherence interval is used for channel estimation for large K , degrading the spectral and energy efficiencies.

B. Proposed Method

For the efficient use of resources and exploiting the spatial diversity, unlike the silent protocol [16], [18]–[20], [26], [27], we assume that all the tags simultaneously reflect pilot symbols during the estimation phase. For the considered network (Fig. 2), we design a pilot protocol to estimate $\bar{\mathbf{H}} = [\mathbf{h}_0, \sqrt{\alpha} \mathbf{h}_1, \dots, \sqrt{\alpha} \mathbf{h}_K]$ in one-shot. The tags are simple, passive devices with a fixed reflection coefficient, α . We assume that the reader knows the value of α . This assumption is consistent with the prior studies [16], [18]–[20], [26], [27]. However, it is noteworthy to mention the pilot sequence design is independent of factors such as α or the channel statistical model. Moreover, if tags have unequal reflection coefficients, denoted as α_k for $k \in \mathcal{K}$, the columns of $\bar{\mathbf{H}}$ to be estimated will be $\sqrt{\alpha_k} \mathbf{h}_k$ for $k \in \mathcal{K}$. As long as the reader has the knowledge α_k , it can estimate the cascaded channels, \mathbf{h}_k , by removing the effect of α_k .

Consequently, the received signal at the reader over τ pilot symbols, $\mathbf{Y} \in \mathbb{C}^{M \times \tau}$, is given as

$$\mathbf{Y} = \sqrt{p} \mathbf{h}_0 \mathbf{s} + \sqrt{p\alpha} \sum_{i \in \mathcal{K}} \mathbf{h}_i (\mathbf{s} \odot \mathbf{c}_i) + \mathbf{N}, \quad (3)$$

where $\mathbf{c}_i = [c_{i1}, \dots, c_{i\tau}]$ is the i -th tag pilot sequence, and c_{ij} is the modulated symbol of the i -th tag in the j -th slot. Moreover, $\mathbf{N} \in \mathbb{C}^{M \times \tau}$ is the noise matrix with i.i.d $\mathcal{CN}(0, \sigma^2)$ elements. By defining $\mathbf{S} \triangleq \text{diag}(\mathbf{s})$, we can rewrite the received signal at the reader (3) as follows:

$$\mathbf{Y} = \sqrt{p} \mathbf{h}_0 \mathbf{1}_\tau \mathbf{S} + \sqrt{p\alpha} \sum_{i \in \mathcal{K}} \mathbf{h}_i \mathbf{c}_i \mathbf{S} + \mathbf{N}, \quad (4)$$

where $\mathbf{1}_\tau \triangleq [1, \dots, 1] \in \mathbb{R}^{1 \times \tau}$ is the all-1 sequence. From (4), we can see that the RF source acts as a hidden tag with an all-1 pilot sequence. Hence, the simple assignment of orthogonal pilot sequences to the tags is not sufficient to prevent pilot contamination. Specifically, even for a mutually set of orthogonal tag pilot sequences, if they are not orthogonal to the all-1 sequence, the direct channel and the cascaded channels can not be separated at the reader. Hence, this is somewhat akin to pilot contamination, which appears in multi-cell networks when pilots are reused in adjacent cells. As in conventional networks, this leads to corrupted channel estimates (Section III-A).

Theorem 1. To avoid pilot contamination, T_k 's pilot sequence must satisfy the following conditions:

- 1) To avoid interference from the RF source

$$\mathbf{1}_\tau \mathbf{c}_k^H = 0, \quad (5)$$

- 2) To avoid interference from the other tags

$$\mathbf{c}_i \mathbf{c}_k^H = 0, \quad (6)$$

where $i \in \mathcal{K}_k$.

The RF source serves a dual role: it transmits the RF signal allowing tags to backscatter data/pilots to the reader while also behaving as a concealed tag itself. Essentially, it functions as an additional tag emitting an all-1 pilot sequence. It is essential to consider this aspect when designing optimal pilot schemes.

Next, the received signal (4) is transformed into a matrix form as

$$\mathbf{Y} = \sqrt{p}\bar{\mathbf{H}}\mathbf{X}\mathbf{S} + \mathbf{N}, \quad (7)$$

where

$$\mathbf{X} = \begin{bmatrix} 1 & 1 & 1 & \cdots & 1_\tau \\ c_{11} & c_{12} & c_{13} & \cdots & c_{1\tau} \\ c_{21} & c_{22} & c_{23} & \cdots & c_{2\tau} \\ \vdots & \vdots & \vdots & \ddots & \vdots \\ c_{K1} & c_{K2} & c_{K3} & \cdots & c_{K\tau} \end{bmatrix}. \quad (8)$$

This signal, \mathbf{Y} , can be further written as

$$\mathbf{y} = \mathbf{A}\bar{\mathbf{h}} + \mathbf{n}, \quad (9)$$

where $\mathbf{y} \in \mathbb{C}^{M\tau \times 1}$, $\bar{\mathbf{h}} = \text{vec}(\bar{\mathbf{H}}) \in \mathbb{C}^{M(K+1) \times 1}$, and $\mathbf{A} = \text{diag}([\sqrt{p}s_1 \mathbf{1}_M, \dots, \sqrt{p}s_\tau \mathbf{1}_M])(\mathbf{X}^T \otimes \mathbf{I}_M) \in \mathbb{C}^{M\tau \times M(K+1)}$. Besides, $\mathbf{n} \sim \mathcal{CN}(\mathbf{0}, \sigma^2 \mathbf{I}_{M\tau})$.

Based upon the linear model (9), we derive the MVU estimator of $\bar{\mathbf{h}}$, which provides the sufficient design criterion for \mathbf{X} , such that the variance of the estimator is minimized.

Theorem 2. For the linear model (9), with unknown deterministic variable $\bar{\mathbf{h}}$, complex Gaussian noise, i.e., $\mathbf{n} \sim \mathcal{CN}(\mathbf{0}, \sigma^2 \mathbf{I}_{M\tau})$, and $\tau \geq K + 1$, the MVU estimator of the channel state $\bar{\mathbf{h}}$ is obtained as

$$\hat{\bar{\mathbf{h}}} = (\mathbf{A}^H \mathbf{A})^{-1} \mathbf{A}^H \mathbf{y}, \quad (10)$$

which is efficient and attains the CRLB, which is a lower bound for the variance of any unbiased estimator [36]. And the estimation variance is minimized when $\mathbf{X}\mathbf{X}^H = \tau \mathbf{I}_{K+1}$. The covariance matrix is thus obtained as

$$\mathbf{C}_{\hat{\bar{\mathbf{h}}}} = \frac{\sigma^2}{p\tau} \mathbf{I}_{M(K+1)}, \quad (11)$$

where the estimation variance for each element of $\hat{\bar{\mathbf{h}}}$ is $\sigma^2/(p\tau)$. Therefore, increasing τ will decrease the variance of the estimates which in turn improves the estimation accuracy.

Proof. See Appendix A. \blacksquare

Remark 2. For the linear model, (9), the MVU estimator (10) has the identical functional form as the LS estimator, which attempts to minimize the squared distance between the given data \mathbf{y} and the unknown variable $\bar{\mathbf{h}}$ [36, Section 14.3.5] (Section III-E).

Theorem 2 leads to the following theorem for a general BackCom network.

Theorem 3. For the BackCom network with K tags (Fig. 2), in order to estimate $\bar{\mathbf{H}} = [\mathbf{h}_0, \sqrt{\alpha}\mathbf{h}_1, \dots, \sqrt{\alpha}\mathbf{h}_K]$, by projecting the received signal (7) onto \mathbf{S}^H , the post-processed received signal is written as

$$\mathbf{Y}' = \sqrt{p}\bar{\mathbf{H}}\mathbf{X} + \mathbf{N}', \quad (12)$$

where $\mathbf{N}' = \mathbf{N}\mathbf{S}^H$ and $\mathbf{X} \in \mathbb{C}^{(K+1) \times \tau}$ contains the signals of the tags with the first row $\mathbf{1}_\tau$, satisfying $\mathbf{X}\mathbf{X}^H = \tau \mathbf{I}_{K+1}$, and $\mathbf{N}' \in \mathbb{C}^{M \times \tau}$ is the noise matrix with i.i.d $\mathcal{CN}(0, \sigma^2)$ elements.

Remark 3. Theorem 3 suggests that a tag should not be assigned with sequence $\mathbf{1}_\tau$, which must be always assigned to the RF source. By doing that, the RF source is essentially treated as a hidden tag. The tags are then assigned mutual orthogonal sequences that are also orthogonal to $\mathbf{1}_\tau$. This strategy is different from pilot assignments to the users in conventional links, where any set of mutually orthogonal sequences can be used by the given users. Clearly, that does not work with the estimation of the direct link and the cascaded channels in BackCom networks.

Remark 4. When $R_b < R_s$, i.e., $R_b = \tau' R_s$, each tag backscatter a symbol $c_k, \forall k$ over τ' symbols of the RF source pilot signal, where τ' is an integer and $\tau' > 1$ [9]. Therefore, the effect of the rate inequality only appears in the matrix \mathbf{S} (7). Thus, in order to create matrix \mathbf{X} , $\tau\tau'$ samples of the RF source signal will be required which ultimately increases the received power, thereby improving the MSEs.

C. Tag Pilot Sequence Designs

We now present several \mathbf{X} choices that meet the design criteria in Theorem 3. These pilot sequence sets have varying levels of complexity. Depending on the processing capability of the tag and the application environment, any of the following sequences may be adopted for BackCom channel estimation.

1) **Hadamard Matrix:** One choice for \mathbf{X} to satisfy the design constraints is the rows of the Hadamard matrix. Specifically, \mathbf{X} can be the first $K + 1$ rows of a Hadamard matrix of order m , i.e., $\mathbf{H}_m^h \in \{1, -1\}^{m \times m}$, where $m = 2^q$ and $q \geq 1$, satisfying $m \geq K + 1$ [37]. Thus, for the channel estimation, $\tau = m$. Note that the assigned pilot sequences of the tags must not contain the all-1 sequence. Hence, when assigning pilot sequences for the tag using the Hadamard matrix, the first row should be excluded. For instance, when there are two tags, i.e., $K + 1 = 3$, we have $m = \tau = 4$ and \mathbf{X} is the first three rows of the Hadamard matrix with order 4 (\mathbf{H}_4^h), given as (13). Thereby, the second and third rows of \mathbf{H}_4^h are assigned to the tags.

$$\mathbf{X} = \begin{bmatrix} 1 & 1 & 1 & 1 \\ 1 & -1 & 1 & -1 \\ 1 & 1 & -1 & -1 \end{bmatrix} \quad (13)$$

2) **Modified ZC Sequences:** ZC sequences have/are been used for downlink (synchronization) and uplink (random access) and reference symbols (pilots) for channel estimation in Long-Term Evolution (LTE) and is a fifth-generation (5G) new radio (NR) [38]. A ZC sequence has two key parameters, (i) the root index $q = \{1, \dots, \tau - 1\}$, and (ii) the length of the sequence, τ , which must be odd and often prime. The q -th ZC sequence, $\mathbf{z}_q = [z_q(0), \dots, z_q(\tau - 1)]$, is defined as

$$z_q(n) = \exp\left(-j\pi q \frac{n(n+1)}{\tau}\right), \quad \text{for } 0 \leq n \leq \tau - 1. \quad (14)$$

These have the desirable constant amplitude and zero auto-correlation properties [38], i.e., (i) $|z_q(n)| = 1$ and (ii) each is orthogonal with cyclically-shifted versions of itself.

However, the ZC sequences do not satisfy the design criteria for backscatter tags in Theorem 1, i.e., $\mathbf{1}_\tau \mathbf{z}_q^H \neq 0$ for $q = \{0, \dots, \tau - 1\}$. Hence, we next propose modified ZC sequences.

Theorem 4. Let $\mathbf{z}_k \in \mathbb{C}^{1 \times \tau}$ for $k \in \mathcal{K}_0$ be any set of orthogonal sequences, i.e., $\mathbf{z}_k \mathbf{z}_{k'}^H = 0$ for $k \neq k'$. To use these in BackCom channel estimation, all the sequences must be orthogonal to the all-1 sequence, i.e., $\mathbf{1}_\tau \mathbf{z}_k^H = 0$ for $k \in \mathcal{K}_0$. However, since this condition does not hold generally for any set of orthogonal sequences, we modify them to satisfy the constraint as follows:

- **Step 1:** Select, say, \mathbf{z}_0 , for convenience.
- **Step 2:** Construct the matrix \mathbf{Q} as follows:

$$\mathbf{Q} \triangleq (\text{diag}(\mathbf{z}_0))^{-1}. \quad (15)$$

- **Step 3:** Use the \mathbf{Q} matrix to modify all other sequences as

$$\mathbf{c}_k = \mathbf{z}_k \mathbf{Q}, \quad \text{for } k \in \mathcal{K}. \quad (16)$$

The modified version of \mathbf{z}_k , i.e., \mathbf{c}_k , satisfies the necessary condition $\mathbf{1}_\tau \mathbf{c}_k^H = 0$ for $k \in \mathcal{K}$. Hence, any set of orthogonal sequences can be modified to satisfy the optimal design criteria (Theorem 1) for BackCom channel estimation.

Following Theorem 4, we adopt modified ZC sequences for BackCom channel estimation.

Example 2. Length 5 ZC sequences: For $K = 3$, we consider $\tau = 5$ and $q = 1$. This gives a ZC sequence

$$\mathbf{z}_0 = [1, e^{-j\frac{2\pi}{5}}, e^{-j\frac{6\pi}{5}}, e^{-j\frac{2\pi}{5}}, 1]. \quad (17)$$

One can readily generate the sequences, i.e., $\mathbf{z}_1, \dots, \mathbf{z}_5$, by performing cyclically-shift as follows:

$$\mathbf{z}_1 = [1, 1, e^{-j\frac{2\pi}{5}}, e^{-j\frac{6\pi}{5}}, e^{-j\frac{2\pi}{5}}], \quad (18a)$$

$$\mathbf{z}_2 = [e^{-j\frac{2\pi}{5}}, 1, 1, e^{-j\frac{2\pi}{5}}, e^{-j\frac{6\pi}{5}}], \quad (18b)$$

$$\mathbf{z}_3 = [e^{-j\frac{6\pi}{5}}, e^{-j\frac{2\pi}{5}}, 1, 1, e^{-j\frac{2\pi}{5}}], \quad (18c)$$

$$\mathbf{z}_4 = [e^{-j\frac{2\pi}{5}}, e^{-j\frac{6\pi}{5}}, e^{-j\frac{2\pi}{5}}, 1, 1], \quad (18d)$$

which are mutually orthogonal. Next, we define $\mathbf{Q} = (\text{diag}(\mathbf{z}_0))^{-1}$. We then construct the pilot sequence of T_k as

$$\mathbf{c}_k = \mathbf{z}_k \mathbf{Q}, \quad \text{for } k = \{1, \dots, 4\}. \quad (19)$$

Therefore, the matrix \mathbf{X} is given as

$$\mathbf{X} = \begin{bmatrix} 1 & 1 & 1 & 1 & 1 \\ e^{-j\frac{2\pi}{5}} & e^{-j\frac{4\pi}{5}} & e^{j\frac{4\pi}{5}} & e^{j\frac{2\pi}{5}} & 1 \\ e^{-j\frac{6\pi}{5}} & 1 & e^{j\frac{6\pi}{5}} & e^{j\frac{2\pi}{5}} & e^{-j\frac{2\pi}{5}} \\ e^{-j\frac{2\pi}{5}} & e^{j\frac{2\pi}{5}} & e^{j\frac{6\pi}{5}} & 1 & e^{-j\frac{6\pi}{5}} \end{bmatrix}, \quad (20)$$

and it can be readily checked that $\mathbf{1}_5(\mathbf{c}_k)^H = 0$.

3) **DFT Matrix:** The rows of DFT matrix [39] can also be used to design the mutual orthogonal sequences of the tags, where $\tau \geq K + 1$.

$$\mathbf{X} = \begin{bmatrix} 1 & 1 & \dots & 1_\tau \\ 1 & W_\tau & \dots & W_\tau^{\tau-1} \\ \vdots & \vdots & \ddots & \vdots \\ 1 & W_\tau^K & \dots & W_\tau^{(\tau-1)K} \end{bmatrix}, \quad (21)$$

where $W_\tau = e^{j2\pi/\tau}$.

The Hadamard matrix is a fundamental orthogonal sequence design, comprised solely of 1s and -1s. Its versatile applications span across modern telecommunications and digital signal processing, encompassing error control coding, Walsh functions, and the generation of spread spectrum signals in CDMA [40]. In contrast to Hadamard sequences, ZC sequences possess a more intricate structure, characterized by unit amplitude and arbitrary phase components. These sequences are crafted from specific phase shifts of unit amplitude complex exponentials [38]. Their prominence arises from a set of highly desirable properties, Section II-B of [38]. ZC sequences find pivotal roles in the LTE standard and 5G NR, contributing significantly to crucial functions such as initial downlink synchronization, random access, uplink control information, and the generation of uplink reference signals (pilot signals). Similarly, the Discrete Fourier Transform (DFT) matrix also exhibits a complex-valued structure with unit amplitude, and it finds wide-ranging applications in the realms of frequency analysis, rapid convolution, and image processing [41]. Furthermore, the DFT matrix plays a pivotal role in designing pilot signals for channel estimation purposes [42] and [39].

Compared to the Hadamard matrix, modified ZC sequences and DFT designs can potentially reduce channel estimation duration (τ), contingent upon the number of devices. However, this reduction comes at the cost of increased complexity for tags, owing to the intricate impedance switching necessary for load modulation [3], [4]. Consequently, these orthogonal sequence types necessitate more intricate RF designs. While passive tags, constrained by energy and processing limitations, may not support such complex pilot sequence designs, tags equipped with greater processing capabilities and sophisticated front-end RF circuits—namely, active and semi-passive tags—can leverage these sequences for diverse applications.

In summary, Table II provides an overview of the properties and requirements associated with the proposed sequence designs.

D. Advantages of the Proposed Method

- The cascade channels $f_k \mathbf{g}_k$ for $k \in \mathcal{K}$ and direct channel \mathbf{h}_0 are estimated simultaneously.
- The cascaded channels are estimated directly, avoiding error propagation.
- The orthogonality across the $K+1$ estimations is ensured. This is done by treating the RF source as a hidden tag to whom an all-1 sequence is assigned.
- Each channel estimate is computed over all time slots, τ . Following Theorem 2, this approach will thus achieve $\sigma^2/(\tau p)$ variance for direct and cascaded channel coefficients. Whereas, in the silent protocol, the variance is $\sigma^2(K+1)/(\tau p)$. Hence, our method can use shorter pilot sequences compared to the silent protocol and yet achieve the performance of long pilot sequences.

Fig. 5 provides a summary of our proposed scheme.

TABLE II: Pilot sequence designs.

Sequence design (\mathbf{X})	Duration (τ)	Tag's complexity
Hadamard matrix	$\tau = m (\geq K + 1)$ (order of Hadamard matrix)	Simple RF design
Modified ZC sequences	$\tau \geq K + 1$ (an odd and often prime number)	Complex impedance switching
DFT matrix	$\tau \geq K + 1$	Complex impedance switching

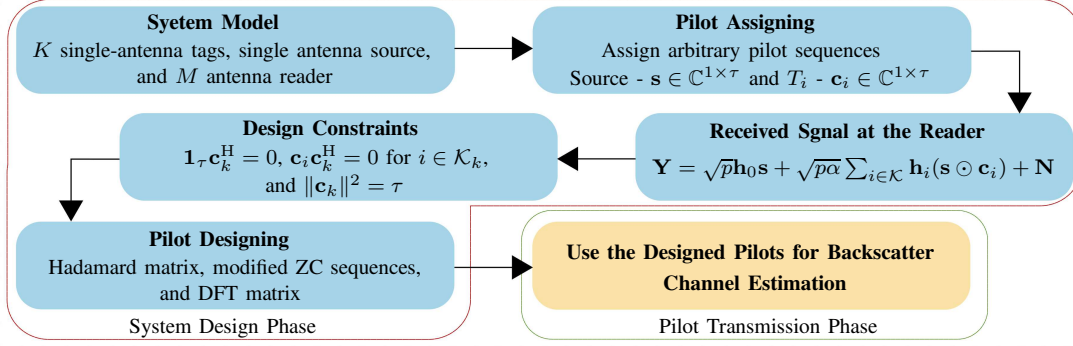


Fig. 5: The proposed channel estimation protocol.

E. Deterministic & Bayesian Channel Estimators

Next, we derive multiple channel estimators, encompassing deterministic methods (LS and scaled LS) and Bayesian approaches (MMSE and LMMSE). It is important to note that the deterministic estimators assume an unknown yet deterministic channel matrix, while Bayesian estimators require the knowledge of prior probability distribution of the channels [36]. Thus, MMSE and LMMSE estimators leverage prior knowledge of channel statistics to enhance estimation accuracy. We define the pilot-symbol matrix as $\bar{\mathbf{X}} = \sqrt{p}\mathbf{X}$, which is predetermined and known to the reader. These estimators of \mathbf{H} can then be expressed as follows [39]:

- 1) **LS channel estimator:** This can be obtained by using (12) as follows:

$$\hat{\mathbf{H}}_{\text{LS}} = \mathbf{Y}'\bar{\mathbf{X}}^\dagger, \quad (22)$$

where $\bar{\mathbf{X}}^\dagger = \bar{\mathbf{X}}^H(\bar{\mathbf{X}}\bar{\mathbf{X}}^H)^{-1}$. Its versatility and effectiveness, along with its ability to function without prior channel knowledge, make this suitable for various applications.

- 2) **Scaled LS channel estimator:** The LS estimate (22) may not always yield the minimum MSE [39]. A solution is to optimally scale the LS channel estimate to further reduce the MSE by allowing for a bias. This estimator is given as (Appendix B)

$$\hat{\mathbf{H}}_{\text{SLS}} = \gamma_0 \hat{\mathbf{H}}_{\text{LS}}, \quad (23)$$

where $\gamma_0 = \text{Tr}\{\mathbf{R}_{\hat{\mathbf{H}}_{\text{LS}}}\} / (\sigma^2 M \text{Tr}\{(\bar{\mathbf{X}}\bar{\mathbf{X}}^H)^{-1}\} + \text{Tr}\{\mathbf{R}_{\hat{\mathbf{H}}_{\text{LS}}}\})$, in which $\text{Tr}\{\mathbf{R}_{\hat{\mathbf{H}}_{\text{LS}}}\} = \text{Tr}\{\hat{\mathbf{H}}_{\text{LS}}^H \hat{\mathbf{H}}_{\text{LS}}\}$. This achieves a lower MSE than the LS estimator [39].

- 3) **MMSE channel estimator:** This is designed to minimize the MSE. The reader implements it by correlating the post-processed received signal in (12) with \mathbf{X} [43], [44], which results in a de-spreading operation. The output signal of this operation is thus given as

$$\mathbf{Y}_p = \mathbf{Y}'\mathbf{X}^H/\tau = \sqrt{p}\bar{\mathbf{H}} + \mathbf{N}_p, \quad (24)$$

where $\mathbf{N}_p = \mathbf{N}'\mathbf{X}^H/\tau$ having i.i.d $\mathcal{CN}(0, \sigma_p^2)$ elements, where $\sigma_p^2 = \sigma^2/\tau$. Given independent Nakagami- \bar{m} fading, the elements of the channel matrix and the noise matrix are statistically independent. Next, the (m, k) -th element of (24) is given as

$$[\mathbf{Y}_p]_{m,k} \triangleq y_{m,k} = \sqrt{p}\bar{h}_{m,k} + n_{m,k}, \quad (25)$$

where $\bar{h}_{m,k} = [\bar{\mathbf{H}}]_{m,k}$, and $n_{m,k} = [\mathbf{N}_p]_{m,k}$. This estimator thus becomes (Appendix C)

$$\begin{aligned} \hat{h}_{m,k} &= \mathbb{E}\{\bar{h}_{m,k}|y_{m,k}\} = \frac{\mathbb{E}\{\bar{h}_{m,k}y_{m,k}^*\}}{\mathbb{E}\{|y_{m,k}|^2\}} y_{m,k} \\ &= \begin{cases} \frac{\sqrt{p}\beta_{m0}}{p\beta_{m0} + \sigma_p^2} y_{m0}, & \text{for } k = 0, \\ \frac{\sqrt{\alpha p}\beta_{mk}}{\alpha p\beta_{mk} + \sigma_p^2} y_{mk}, & \text{for } k \in \mathcal{K}, \end{cases} \end{aligned} \quad (26)$$

where $\beta_{m,k}$ is given as

$$\beta_{m0} = \frac{\Gamma(\bar{m}_{h_0} + 1) \Omega_{h_0}}{\Gamma(\bar{m}_{h_0}) \bar{m}_{h_0}}, \quad (27a)$$

$$\beta_{mk} = \frac{\Gamma(\bar{m}_{f_k} + 1)\Gamma(\bar{m}_{g_{mk}} + 1) \Omega_{f_k} \Omega_{g_{mk}}}{\Gamma(\bar{m}_{f_k})\Gamma(\bar{m}_{g_{mk}}) \bar{m}_{f_k} \bar{m}_{g_{mk}}}. \quad (27b)$$

The estimate of T_k 's effective channel, i.e., $\hat{\mathbf{h}}_k$, is then given as $\hat{\mathbf{h}}_k = \sqrt{\gamma_k}\mathbf{y}_k$, where \mathbf{y}_k is the k -th column of \mathbf{Y}_p , and $\gamma_k = \frac{\alpha p\beta_k^2}{\alpha p\beta_k + \sigma_p^2}^{-1}$ [45]. Thus, the estimate of the complete channel matrix, $\bar{\mathbf{H}}$, is given as

$$\hat{\mathbf{H}}_{\text{MMSE}} = \mathbf{Y}_p \mathbf{D}_\gamma^{1/2}, \quad (28)$$

where $\mathbf{D}_\gamma = \text{diag}([\gamma_0, \gamma_1, \dots, \gamma_K])$ and $\gamma_0 = \frac{p\beta_0^2}{p\beta_0 + \sigma_p^2}$.

- 4) **LMMSE channel estimator:** This estimator is sub-optimal but offers an ease of implementation. Using (24), the received signal from the direct channel and the cascaded channels will take the form

$$\mathbf{y}_{p,k} = \sqrt{p}\bar{\mathbf{h}}_k + \mathbf{n}_{p,k}, \quad \text{for } k \in \mathcal{K}_0, \quad (29)$$

¹Note that since the reader has co-located antennas, $\beta_{mk} = \beta_k$ for $m \in \mathcal{M}$.

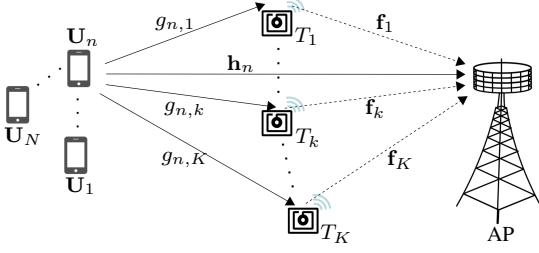


Fig. 6: Cellular-based passive/ambient IoT network.

where $\mathbf{y}_{p,k}$, $\bar{\mathbf{h}}_k$ and $\mathbf{n}_{p,k}$ are respectively the k -th column of \mathbf{Y}_p , $\bar{\mathbf{H}}$ and \mathbf{N}_p . Therefore, the LMMSE estimation of $\hat{\mathbf{h}}_k$ is expressed as (Proof [36, Theorem 12.1])

$$\hat{\mathbf{h}}_k = \mathbb{E}\{\bar{\mathbf{h}}_k\} + \sqrt{p}\mathbf{C}_{\bar{\mathbf{h}}_k} (p\mathbf{C}_{\bar{\mathbf{h}}_k} + \sigma_p^2\mathbf{I}_M)^{-1} \times (\mathbf{y}_{p,k} - \sqrt{p}\mathbf{I}_M\mathbb{E}\{\bar{\mathbf{h}}_k\}). \quad (30)$$

Remark 5. While this focuses on AmBC, we stress that our method can also be applied to MoBC, BiBC, and integrated BackCom that combines legacy networks (such as SR [9]) with newer ones. Our method can accommodate these different configurations in Figure 1. Specifically, for MoBC, with co-located RF source and reader, the direct link disappears, removing the constraints due to all-1 sequence.

IV. MULTIPLE-USER MULTIPLE-TAG SCENARIO

We next present an extension of our proposed channel estimation scheme to handle multiple tags and multiple users (Fig. 6). This setup comprises cellular-based passive/ambient IoT networks where multiple tags operate in the presence of multiple users. It can apply to SR networks, ambient IoT, passive IoT, and others. Such networks may find applications in smart homes, smart cities, industrial IoT, and healthcare [1]–[3].

We thus consider a network comprising an M -antenna RF source, e.g., AP, N single-antenna users, i.e., \mathbf{U}_n for $n \in \mathcal{N}$, and K single-antenna tags, i.e., T_k for $k \in \mathcal{K}$, as shown in Fig. 6. Here, we will have one set of orthogonal sequences assigned to the users (e.g., pilots used for cellular users) and a subset of orthogonal sequences for a given user, which are assigned to the tags, treating the user as a hidden tag. We denote the channels between \mathbf{U}_n and the AP, \mathbf{U}_n and T_k , and T_k and the AP as $\mathbf{h}_n \in \mathbb{C}^{M \times 1}$, $g_{n,k} \in \mathbb{C}$, and $\mathbf{f}_k \in \mathbb{C}^{M \times 1}$, respectively, for $n \in \mathcal{N}$ and $k \in \mathcal{K}$.

In the following, we assume that the data rate of a tag is lower than that of the AP, i.e., the tag backscatter one symbol over τ' symbols of the AP ($R_s = \tau' R_b$ - Remark 4).

Suppose that the channel estimation phase comprises Q time slots. In the i -th time slot, the users send mutual orthogonal pilot sequences, $\sqrt{\tau'}\mathbf{s}_n \in \mathbb{C}^{1 \times \tau'}$, where $\|\mathbf{s}_n\|^2 = 1$ and $\tau' \geq N$. Besides, $\mathbf{s}_n\mathbf{s}_{n'}^H = 0$ for $(n \neq n')$. Meanwhile, each tag backscatters a symbol, i.e., $c_k, \forall k$, over the users' pilot signals, $\mathbf{s}_n, \forall n$.

The received signal at the AP over the i -th time slot is thus

$$\mathbf{Y}_i = \sqrt{\tau'p} \sum_{n \in \mathcal{N}} \bar{\mathbf{H}}_n \mathbf{x}_i \mathbf{s}_n + \mathbf{N}_i, \quad (31)$$

TABLE III: Simulation settings.

Parameter	Value	Parameter	Value
f_c	3 GHz	d_{n_0}	10 m
B	10 MHz	$d_{f_k}, k \in \mathcal{K}$	$\mathcal{U}(5, 7)$ m
N_f	20 dB	$d_{g_k}, k \in \mathcal{K}$	6 m
\bar{m}	3	M	10

where $\bar{\mathbf{H}}_n = [\mathbf{h}_n, \alpha \mathbf{f}_1 g_{n,1}, \dots, \alpha \mathbf{f}_K g_{n,K}]$, $\mathbf{x}_i = [1, c_1, c_2, \dots, c_K]^T \in \mathbb{C}^{(K+1) \times 1}$, and $\mathbf{N}_i \in \mathbb{C}^{M \times \tau'}$ is the AWGN matrix at the AP with i.i.d $\mathcal{CN}(0, \sigma^2)$ elements.

To estimate channels, the received pilot signal at the AP (31) is projected onto \mathbf{s}_n^H for $n \in \mathcal{N}$ which yields [43], [44]

$$\tilde{\mathbf{y}}_{n,i}^p = \sqrt{\tau'p} \bar{\mathbf{H}}_n \mathbf{x}_i + \tilde{\mathbf{n}}_{i,n}, \quad (32)$$

where $\tilde{\mathbf{n}}_{i,n} = \mathbf{N}_i \mathbf{s}_n^H \sim \mathcal{CN}(\mathbf{0}, \sigma^2 \mathbf{I}_M)$.

Using (32), it is crucial to create matrix $\mathbf{X} = [\mathbf{x}_1, \dots, \mathbf{x}_i, \dots, \mathbf{x}_Q] \in \mathbb{C}^{(K+1) \times Q}$ (Theorem 3) to enable the reader to estimate the direct channel and cascaded channels per user. Hence, at least $K+1$ slots are required, i.e., $Q \geq K+1$. Therefore, using (32), the received signal over Q time slots can be collected as

$$\tilde{\mathbf{Y}}_n^p = \bar{\mathbf{H}}_n \sqrt{\tau'p} \mathbf{X} + \tilde{\mathbf{N}}_n, \quad (33)$$

where $\tilde{\mathbf{N}}_n = [\tilde{\mathbf{n}}_{1,n}, \dots, \tilde{\mathbf{n}}_{Q,n}] \in \mathbb{C}^{M \times Q}$.

The obtained equation in (33) is similar to (12). Following the same principles, Theorem 3, and Section III-C, designs for \mathbf{X} could be the first $K+1$ rows of a Hadamard matrix of order $m \geq K+1$ with $Q = m$, modified ZC sequences, or DFT matrix. Moreover, using (41), the estimation variance for each element of $\bar{\mathbf{H}}_n$ is $\sigma^2 / (p\tau'Q)$, and the duration of the training phase is $\tau = \tau'Q$. Next, from (33), a channel estimator aims to recover $\bar{\mathbf{H}}_n$ for $n \in \mathcal{N}$, by exploiting \mathbf{X} and $\tilde{\mathbf{Y}}_n^p$. Therefore, $\hat{\bar{\mathbf{H}}}_n$ can be obtained using the estimation methods in Section III-E.

V. SIMULATION RESULTS

We next present and discuss extensive simulation and numerical results to validate the proposed estimators. To evaluate their performance, we use a channel model that accounts for both large-scale and small-scale fading, ensuring a realistic representation of the wireless communication environment. Large-scale fading is modeled by the the 3GPP urban micro (UMi), i.e., ζ_a for $a \in \mathcal{A}$, with carrier frequency f_c [46, Table B.1.2.1]. Moreover, the AWGN variance is modeled as $\sigma^2 = 10 \log_{10}(N_0 B N_f)$ dBm, where $N_0 = -174$ dBm/Hz, B is the bandwidth, and N_f is the noise figure. Table III gives the simulation parameters. Unless otherwise specified, we use the Hadamard sequences for performance evaluations. Without loss of generality, we set $\alpha = 0.6$.

We use the linear estimators, i.e., LS (22), scaled LS (23), and LMMSE (30) to estimate the direct channel (\mathbf{h}_0) and the cascaded channels ($f_k \mathbf{g}_k, k \in \mathcal{K}$). Note that the MVU estimator matches the LS estimator in the simulation (Remark 2). To benchmark the performance of our channel estimators, we consider the prior art [17], [19]–[21], [27]. Here, we evaluate the LMMSE estimator with phase-splitting as described in Section III-A.

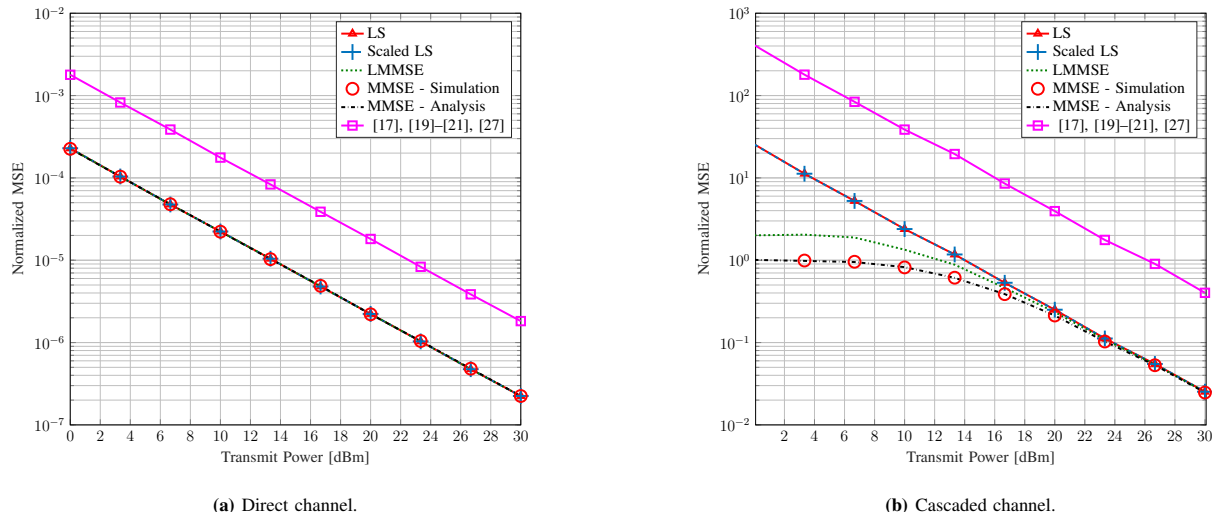


Fig. 7: Channel estimation for $\tau = 8$ and $K = 7$.

The quality of channel estimators is widely assessed in terms of normalized MSE, which is defined as

$$\text{Normalized MSE}_k = \mathbb{E} \left\{ \frac{\|\mathbf{h}_k - \hat{\mathbf{h}}_k\|_2^2}{\|\mathbf{h}_k\|_2^2} \right\}, \quad k \in \mathcal{K}_0, \quad (34)$$

where $\hat{\mathbf{h}}_k$ is the k -th column of $\hat{\mathbf{H}}_\eta$, where $\eta \in \{\text{LS, scaled LS, LMMSE, MMSE}\}$. Note that, the analytical MSE of MMSE estimator (legend MMSE-analysis) is plotted via by substituting $\hat{\mathbf{h}}_k$ in (26) into (34), whereas the simulated MSE of MMSE estimator (legend MMSE-simulation) is plotted by evaluating $[\hat{h}_{m,k}]_{\text{Simulation}} = \mathbb{E}\{\hat{h}_{m,k}|y_{m,k}\}$ through Monte-Carlo simulations to validate the derived analytical expression.

Fig. 7 shows the normalized MSE performance of different estimators versus the transmit power for the direct channel and cascaded channels, for $\tau = 8$ and $K = 7$ tags. With seven tags, the silent method [17], [19]–[21], [27] uses one pilot symbol ($t = 1$) to estimate each channel, i.e., the direct channel \mathbf{h}_0 or the combined channel $\mathbf{h}_0 + \alpha f_k \mathbf{g}_k$ for $k \in \mathcal{K}$.

Our proposed method demonstrates remarkable accuracy in estimating both direct and cascade channels for multiple tag scenarios. It significantly outperforms the silent protocol. Moreover, due to the double path loss in the cascaded channel, it excels at estimating the direct link channel more accurately than the cascaded channel (Fig. 7a and Fig. 7b). Additionally, our linear estimators deliver comparable performance to the optimal MMSE estimator.

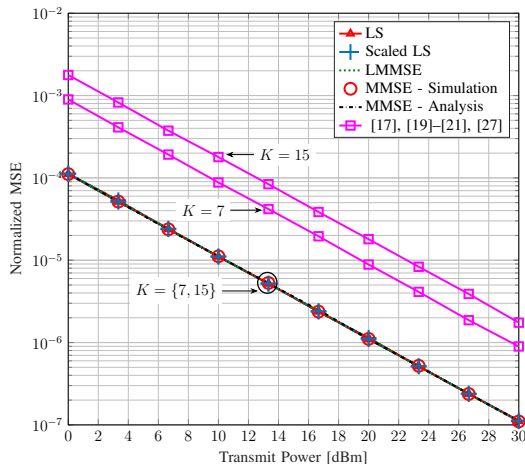
Furthermore, we achieve a normalized MSE of 10^{-5} at 14 dBm transmit power, whereas the silent method [17], [19]–[21], [27] requires 10 dBm more to achieve the same MSE. The primary reason for this massive power savings is that our method utilizes the entire pilot length for each channel while avoiding pilot contamination, whereas the silent case allocates a portion of the pilot sequence to each channel.

It is also worth noting that the traditional LS (or scaled LS) method outperforms the LMMSE estimation method with

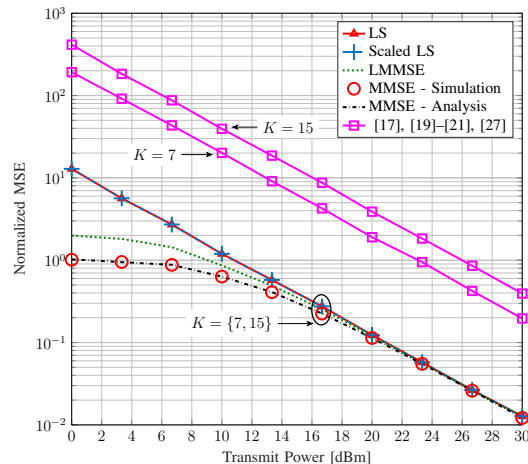
the silent protocol. The estimation quality of all the cascaded channels is almost the same (Fig. 7b), independent of the number of tags. The gap between the proposed method and the silent method using the LMMSE estimator is even larger than that of the direct channel. This is because the silent method suffers from error propagation (Section III-A). In particular, compared to our method, the silent case requires ~ 13 dBm more transmit power to achieve the normalized MSE of 10^{-1} . Moreover, with our method, the simple LS (or scaled LS), significantly outperforms the LMMSE estimation method using the silent method. We note that LS and scale LS achieve the same performance. This is because, for the latter, the scale parameter $\gamma_0 \sim 1$ for our setup. Moreover, the proposed MMSE estimator performs better in the low transmit power regime due to the use of second-order statistics.

Note that the cascaded channel normalized MSE has high values when compared to the direct channel normalized MSE. This is primarily due to the double path loss present in the cascaded channel and the tag's reflection coefficient α .

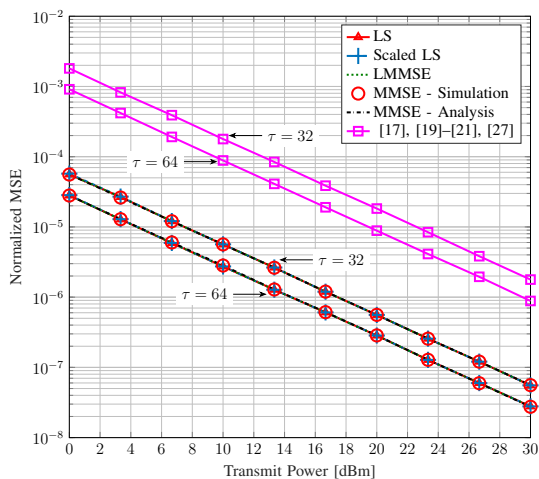
We anticipate a certain relationship between the channel estimation quality and the pilot length, as well as the number of tags. These relationships are uncovered in Fig. 8 and Fig. 9. In Fig. 8, we set $\tau = 16$ and plot the normalized MSE for $K = 7$ and $K = 15$. In particular, Fig. 8a and Fig. 8b investigate the normalized MSE for the direct channel and cascaded channel, respectively. As expected, increasing the number of tags adversely affects the performance of the silent case. In particular, for $K = 15$, the silent case uses one pilot symbol to estimate each of the direct channel and the cascaded ones, while for $K = 7$, it allocated two pilots per link which results in better channel estimates. Therefore, with a large number of tags, the prior art has to use an excessive amount of the channel coherence interval to accurately estimate the channels. On the other hand, our channel estimation proposal achieves the same performance independent of the number of tags for fixed τ , and significantly outperforms the silent case. In particular, for $K = 15$, we observe the power gain of ~ 13 dBm and ~ 16 dBm to achieve the normalized MSE of



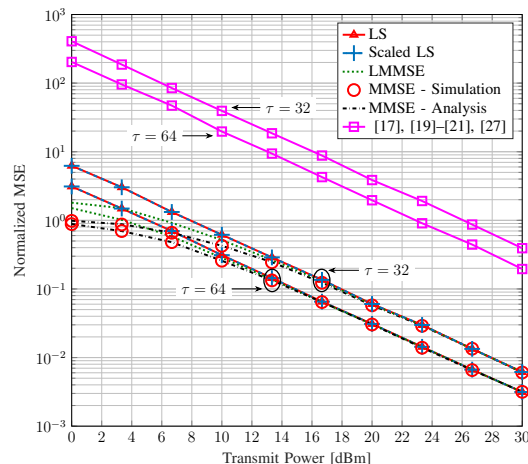
(a) Direct channel.



(b) Cascaded channel.

Fig. 8: Channel estimation for $\tau = 16$ and $K = \{7, 15\}$.

(a) Direct channel.



(b) Cascaded channel.

Fig. 9: Channel estimation for $\tau = \{32, 64\}$ and $K = 31$.

10^{-5} and 10^{-1} for respectively the direct link and cascaded links. Therefore, as the network scales up, our proposed scheme can efficiently handle CSI estimation.

Fig. 9a and Fig. 9b examine the impact of pilot sequence length on the normalized MSE of the channel estimates for a fixed number of tags, $K = 32$. The results show that longer pilot sequences lead to better estimates of the direct and cascaded channels. For example, increasing the pilot sequence length from $\tau = 32$ to $\tau = 64$ results in a transmit power gain of approximately ~ 2.5 dBm for the cascaded channel in the mid-to-high transmit power regime. Furthermore, the proposed scheme outperforms the silent case in terms of normalized MSE, even though both show a similar power gain.

Additionally, Fig. 10a and Fig. 10b plot the normalized MSEs of direct and cascaded channels against the pilot length for $K = 2$ and $p = 20$ dBm. As expected, increasing τ improves the channel estimation accuracy and our method significantly outperforms the prior art. It is worth noting that,

unlike the prior art, our proposal achieves the same accuracy for any number of tags satisfying $\tau \geq K + 1$.

In Fig. 11, we plot the normalized MSE as a function of the number of tags, K , for $\tau = 64$ and $p = 20$ dBm. Since our method is independent of the number of tags, the normalized MSE remains constant, whereas the performance of the silent protocol depends on K . When there is no tag ($K = 0$), our protocol and the silent one have the same normalized MSE because the entire pilot duration is allocated to the direct channel estimation (Fig. 11a). However, as K increases, the silent protocol assigns $\tau/(K + 1)$ estimation time for each channel gain and is plagued by error propagation. For these reasons, the performance gap, G_p , increases (Fig. 11a and Fig. 11b). From numerical experiments, we find that G_p can be modeled as

$$G_p = \lambda_G \tau \left(1 - \frac{1}{K + 1} \right), \quad \text{for } 0 \leq K \leq \tau - 1, \quad (35)$$

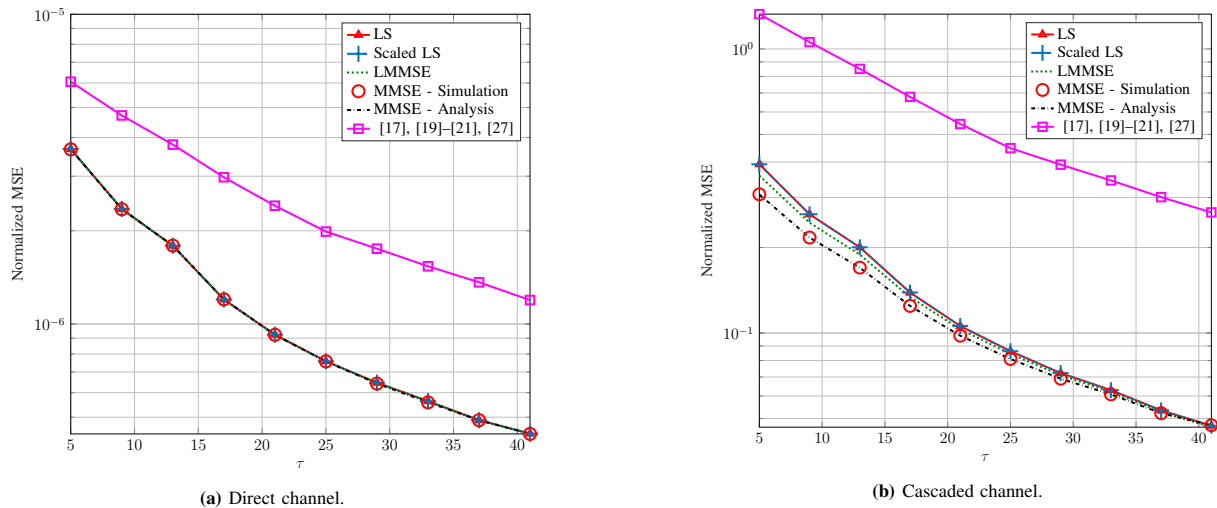


Fig. 10: Channel estimation for $p = 20$ dBm, $K = 2$, and $\alpha = 0.6$.

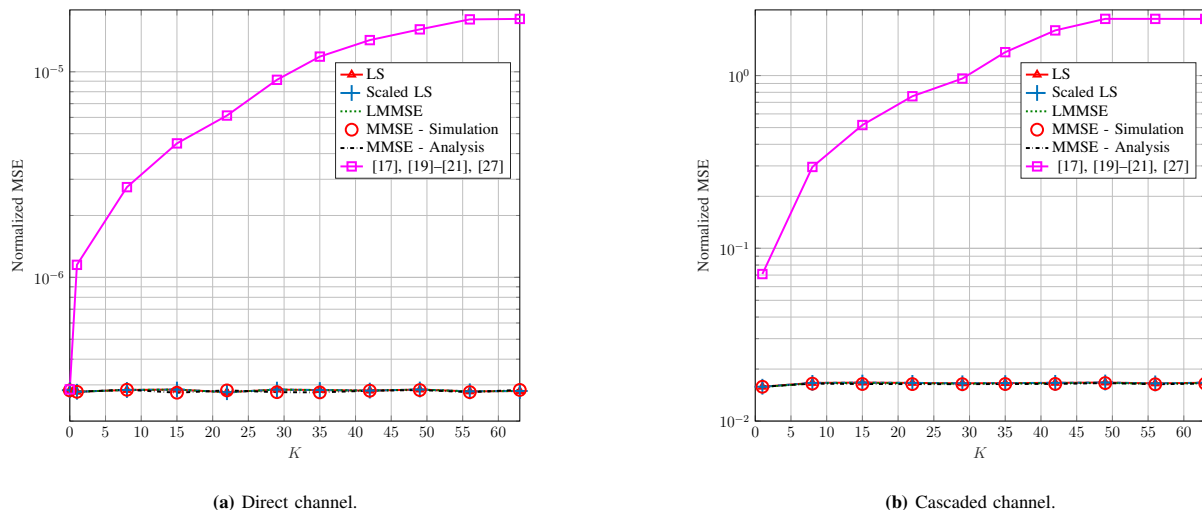


Fig. 11: Channel estimation for $p = 20$ dBm, $\tau = 64$, and $\alpha = 0.6$.

where λ_G accounts for the other system parameters, i.e., transmit power, noise variance, tag's reflection coefficient, etc.

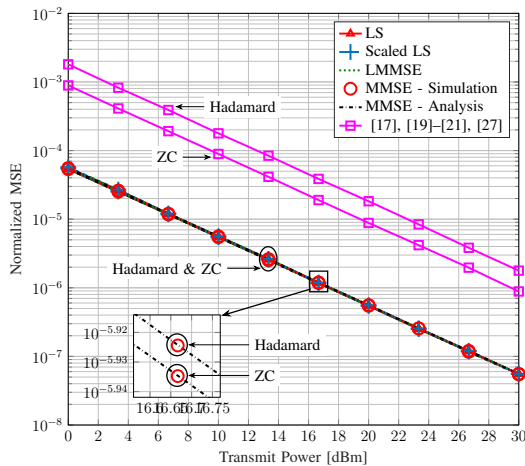
It is interesting to see if different pilot sequences make a difference. To this end, Fig. 12 compares Hadamard and ZC sequences for $K = 32$. To ensure a fair comparison, we choose $\tau = 32$ for Hadamard and $\tau = 33$ for ZC. Consequently, when using the latter in the silent method, the additional pilot is used for direct channel estimation (Fig. 12a), while each cascaded channel is estimated using a single pilot (Fig. 12b). As a result, with the silent protocol, the ZC sequence outperforms the Hadamard sequence in terms of normalized MSE for the direct channel. The proposed channel estimation scheme with the ZC sequence, on the other hand, has slightly better performance in both the direct and cascaded channels, due to the use of one additional pilot symbol (enlarged portions of Fig. 12a and Fig. 12b). Accordingly, the performance of any set of pilot sequences that meet the optimal design criterion - Theorem 3 and Theorem 4 - will be the same for fixed τ .

It is interesting to see if the amount of power reflected by

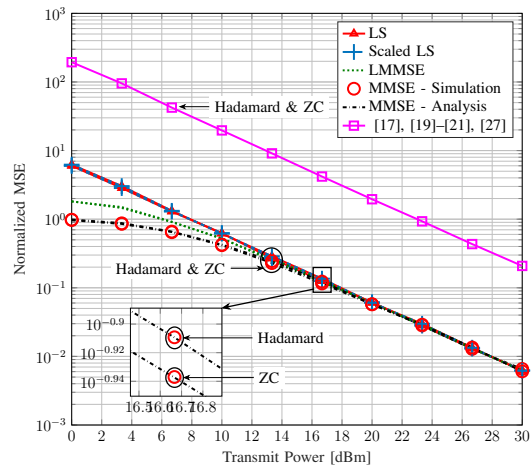
the tags has an impact on the channel estimation quality. We test this possibility in Fig. 13 and consider $\tau = 16$, $K = 7$, with $\alpha = \{0.6, 0.8\}$. The estimation quality of the direct link is independent of α (Fig. 13a). However, for the cascaded links, higher α increases the reflected power at each tag, improving the estimation quality. Nonetheless, α should be set carefully to keep the passive tag functional and maintain a balance between the harvested and the reflected power (Section II-B).

VI. CONCLUSION

The prior solutions to the BackCom channel estimation problem use the silent protocol, where the tags cycle through active and silent periods. It has several, critical drawbacks (Section III-A). In this paper, we have developed a new protocol for the time spreading of tag pilots over the entire estimation interval. It enables the simultaneous estimation of both direct and cascaded links, utilizing the whole training phase for each channel, and avoids error propagation inherent in prior sequential estimation methods. It thus offers remarkable power

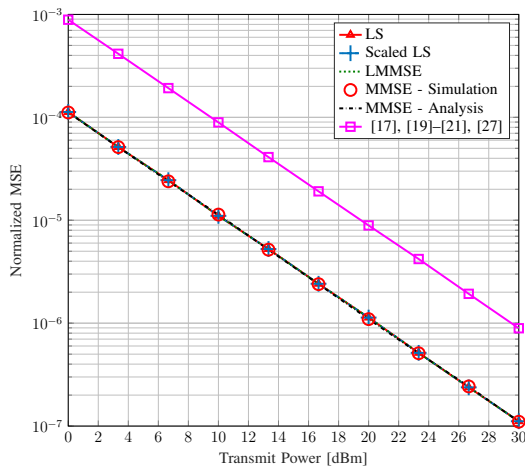


(a) Direct channel.

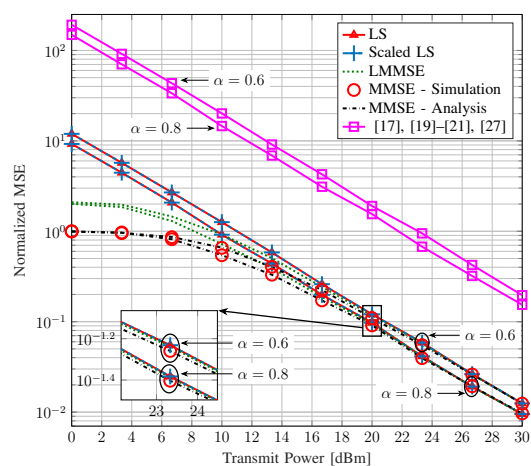


(b) Cascaded channel.

Fig. 12: Performance comparison between Hadamard and ZC sequences for $K = 32$. For Hadamard, $\tau = 32$, and for ZC, $\tau = 33$.



(a) Direct channel.



(b) Cascaded channel.

Fig. 13: Channel estimation for $\tau = 16$, $K = 7$, and $\alpha = \{0.6, 0.8\}$.

reductions of at least 10 dBm (direct) and 12 dBm (cascaded) compared to the silent protocol, respectively (Fig. 7). This gap can be attributed to the following factors: (i) direct estimation of cascaded channels avoids error propagation, (ii) treating the RF source as a hidden tag avoids pilot contamination, and (iii) time-spread pilots utilize time and energy resources efficiently. In contrast to the prior art, the proposed method can readily accommodate any number of tags.

Before discussing the future directions, we summarize the contributions of this study. Having set up the time-spread pilots, we derived the MVU channel estimator and developed the pilot designs to avoid pilot contamination. Using the designs, an analytical MMSE estimator was also derived and exploited for performance evaluations. The proposed method was also extended for cellular-based passive IoT, where multiple tags operate along with multiple cellular users.

The future extensions of this work are multi-faceted and have the potential to significantly enhance the current state of

the research. Firstly, it is essential to perform separate forward, f_k , and backscatter, g_k , channel estimations to facilitate energy beamformer designs for waking up tags and other related applications. While prior work has been limited in investigating this issue, recent research such as [23] has made progress in obtaining the modulus values $|f_k|$ and $|g_k|$. Hence, our proposed technique can further improve the accuracy of these estimates.

Secondly, the quality of channel estimate has an immense effect on backscatter performance analysis (e.g., bit-error rate/symbol error rate, outage probability, and achievable rate) and resource allocation (e.g., beamforming design, reflection coefficient optimization, and others). Hence, the future extensions of this study will include performance analysis and resource allocation frameworks based on the proposed channel estimation technique.

Thirdly, the proposed time-spread pilot-based channel estimation technique can be utilized for RIS and integrated

systems, such as RIS-assisted BackCom, integrated sensing and BackCom, and others. This approach is particularly useful for passive devices that do not generate RF signals, and it has the potential to enhance the efficiency and effectiveness of these systems.

Finally, hardware impairments can also impact the quality of channel estimation. The RF source and reader have RF front-ends that are vulnerable to amplifier non-linearities, in/quadrature -phase imbalance, phase noise, quantization error, etc. [47]–[49]. Antenna impedance mismatching at the tags affects the reflection coefficient and EH. Synchronization/timing errors and hardware impairments have been scarcely investigated. Thus, these challenges inspire further research. Deep learning-based techniques may help in this context [50].

Overall, our channel estimation approach shows great promise in enhancing the accuracy and reliability of BackCom networks, RIS, and other integrated networks. By proposing extensions to this work, we aim to push the boundaries of the current state-of-the-art in this field and facilitate the development of passive tag-based communication solutions.

APPENDIX A

MVU ESTIMATOR FOR LINEAR MODEL

For an estimator of θ , the MSE is defined as [36, Section 2.4]

$$\text{MSE}(\hat{\theta}) = \mathbb{E}\{(\hat{\theta} - \theta)^2\} = \text{Var}(\hat{\theta}) + b^2(\theta), \quad (36)$$

where $b(\theta) = \mathbb{E}\{\hat{\theta}\} - \theta$. Thus, the MSE can be decomposed into bias and variance. An estimator is unbiased if, on average, it yields the true value, $\mathbb{E}\{\hat{\theta}\} = \theta$. Among unbiased estimators, the one with the minimum variance (MVU estimator) is desirable since its variance, $\text{Var}(\hat{\theta})$, is the smallest among all unbiased estimators.

Theorem 5. [36, Theorem 4.1] *If the data observed can be modeled as*

$$\mathbf{y} = \mathbf{D}\boldsymbol{\theta} + \mathbf{w}, \quad (37)$$

where \mathbf{y} is an $N \times 1$ vector of observations, \mathbf{D} is a known $N \times p$ matrix (with $N > p$) with rank p , $\boldsymbol{\theta}$ is a $p \times 1$ vector of parameters to be estimated, and \mathbf{w} is an $N \times 1$ noise vector with PDF $\mathcal{CN}(\mathbf{0}, \sigma^2 \mathbf{I})$, then the MVU estimator is

$$\hat{\boldsymbol{\theta}} = (\mathbf{D}^H \mathbf{D})^{-1} \mathbf{D}^H \mathbf{y}, \quad (38)$$

And the covariance matrix of $\hat{\boldsymbol{\theta}}$ is

$$\mathbf{C}_{\hat{\boldsymbol{\theta}}} = \sigma^2 (\mathbf{D}^H \mathbf{D})^{-1}. \quad (39)$$

For the linear model (37), the MVU estimator attains the CRLB. Therefore, we have $\mathbf{C}_{\hat{\boldsymbol{\theta}}} = \mathcal{I}^{-1}(\boldsymbol{\theta})$, where $\mathcal{I}(\boldsymbol{\theta})$ is the Fisher information matrix, satisfying [36, Theorem 3.2]

$$[\mathbf{C}_{\hat{\boldsymbol{\theta}}}]_{i,i} = [\mathcal{I}^{-1}(\boldsymbol{\theta})]_{i,i} \geq \frac{1}{[\mathcal{I}(\boldsymbol{\theta})]_{i,i}}. \quad (40)$$

And equality holds when $\mathcal{I}^{-1}(\boldsymbol{\theta})$ is diagonal [36, Ex. 3.12].

Using Theorem 5, the MVU estimator of BackCom channels is obtained as (10), and the covariance matrix is given as

$$\begin{aligned} \mathbf{C}_{\hat{\mathbf{h}}} &= \sigma^2 (\mathbf{A}^H \mathbf{A})^{-1} \\ &= \sigma^2 ((\mathbf{X}^T \otimes \mathbf{I}_M)^H \mathbf{B}^H \mathbf{B} (\mathbf{X}^T \otimes \mathbf{I}_M))^{-1} \\ &= \frac{\sigma^2}{p} (\mathbf{X}^{T^H} \mathbf{X}^T \otimes \mathbf{I}_M)^{-1} \\ &= \frac{\sigma^2}{p} (\mathbf{X}^{T^H} \mathbf{X}^T)^{-1} \otimes \mathbf{I}_M, \end{aligned} \quad (41)$$

where $\mathbf{B} = \text{diag}([\sqrt{p}s_1 \mathbf{1}_M, \dots, \sqrt{p}s_\tau \mathbf{1}_M])$.

Using (41), the lower bound in (40) can be attained when $\mathbf{X}\mathbf{X}^H$ is diagonal. This implies \mathbf{X} has equally scaled orthogonal rows, i.e., $\mathbf{X}\mathbf{X}^H = \beta \mathbf{I}_{K+1}$, such that the same variance is achieved for all unknown $\hat{\mathbf{h}}$. Therefore, to minimize the variance of the estimate, β should be maximized under the constraint that the first row of \mathbf{X} is $\mathbf{1}_\tau$ and the remaining elements follow the signal model that can be modulated and reflected by the tags. For $||[\mathbf{X}]_i, j|^2 = 1$, β is found as

$$\beta = \frac{1}{K+1} \text{Tr}(\mathbf{X}\mathbf{X}^H) = \frac{1}{K+1} (K+1)\tau = \tau, \quad (42)$$

and the estimation covariance matrix is obtained as (11).

APPENDIX B

DERIVATION OF SCALED LS ESTIMATOR IN (23)

Following [39, Section IV], we first express channel estimation error as

$$\begin{aligned} &\mathbb{E} \left\{ \|\bar{\mathbf{H}} - \gamma \hat{\mathbf{H}}_{\text{LS}}\|_F^2 \right\} \\ &= \text{Tr} \left(\mathbb{E} \left\{ (\bar{\mathbf{H}} - \gamma \hat{\mathbf{H}}_{\text{LS}})^H (\bar{\mathbf{H}} - \gamma \hat{\mathbf{H}}_{\text{LS}}) \right\} \right) \\ &= (1 - \gamma)^2 \mathbf{R}_{\bar{\mathbf{H}}} + \gamma^2 M \sigma^2 \text{Tr} \left((\bar{\mathbf{X}} \bar{\mathbf{X}}^H)^{-1} \right) \\ &= (J_{\text{LS}} + \text{Tr}(\mathbf{R}_{\bar{\mathbf{H}}})) \left(\gamma - \frac{\text{Tr}(\mathbf{R}_{\bar{\mathbf{H}}})}{J_{\text{LS}} + \text{Tr}(\mathbf{R}_{\bar{\mathbf{H}}})} \right)^2 \\ &\quad + \frac{J_{\text{LS}} \text{Tr}(\mathbf{R}_{\bar{\mathbf{H}}})}{J_{\text{LS}} + \text{Tr}(\mathbf{R}_{\bar{\mathbf{H}}})}, \end{aligned} \quad (43)$$

where $J_{\text{LS}} = \mathbb{E}\{\|\bar{\mathbf{H}} - \hat{\mathbf{H}}_{\text{LS}}\|_F^2\} = M \sigma^2 \text{Tr}((\bar{\mathbf{X}} \bar{\mathbf{X}}^H)^{-1}) = M(K+1)\sigma^2/(\tau p)$, in which $\hat{\mathbf{H}}_{\text{LS}} = \bar{\mathbf{H}} + \mathbf{N}' \bar{\mathbf{X}}^\dagger$, and $\mathbb{E}\{\mathbf{N}'^H \mathbf{N}'\} = M \sigma^2 \mathbf{I}$. Hence, (43) is minimized when

$$\gamma_0 = \frac{\text{Tr}(\mathbf{R}_{\bar{\mathbf{H}}})}{J_{\text{LS}} + \text{Tr}(\mathbf{R}_{\bar{\mathbf{H}}})}, \quad (44)$$

and by using the LS-based consistent sample estimate, i.e., $\text{Tr}(\mathbf{R}_{\hat{\mathbf{H}}})$ instead of $\text{Tr}(\mathbf{R}_{\bar{\mathbf{H}}})$, scaled LS is obtained as (23).

APPENDIX C

DERIVATION OF MMSE ESTIMATOR IN (26)

We first evaluate the expectation term in the numerator as

$$\begin{aligned} \mathbb{E}\{\bar{h}_{m,k} y_{m,k}^*\} &= \mathbb{E}\{\bar{h}_{m,k} (\sqrt{p} \bar{h}_{m,k}^* + n_{m,k}^*)\} \\ &= \sqrt{p} \mathbb{E}\{\bar{h}_{m,k} \bar{h}_{m,k}^*\} + \mathbb{E}\{\bar{h}_{m,k} n_{m,k}^*\} \\ &= \begin{cases} \sqrt{p} \beta_{m0}, & \text{for } k = 0, \\ \sqrt{\alpha p} \beta_{mk}, & \text{for } k \in \mathcal{K}, \end{cases} \end{aligned} \quad (45)$$

where β_{mk} is given in (27a). Next, the expectation term in the denominator is obtained as

$$\begin{aligned} \mathbb{E}\{|y_{m,k}|^2\} &= p\mathbb{E}\{|\bar{h}_{m,k}|^2\} + \mathbb{E}\{|n_{m,k}|^2\} \\ &= \begin{cases} p\beta_{m0} + \sigma_p^2, & \text{for } k = 0, \\ \alpha p\beta_{mk} + \sigma_p^2, & \text{for } k \in \mathcal{K}. \end{cases} \end{aligned} \quad (46)$$

Hence, the MMSE of $\bar{h}_{m,k}$ is given as (26).

REFERENCES

- [1] N. Van Huynh, D. T. Hoang, X. Lu, D. Niyato, P. Wang, and D. I. Kim, "Ambient backscatter communications: A contemporary survey," *IEEE Commun. Surveys Tuts.*, vol. 20, no. 4, pp. 2889–2922, 4th Quart. 2018.
- [2] U. S. Toro, K. Wu, and V. C. M. Leung, "Backscatter wireless communications and sensing in green internet of things," *IEEE Tran. Green Commun. Netw.*, vol. 6, no. 1, pp. 37–55, Mar. 2022.
- [3] D. Galappaththige, F. Rezaei, C. Tellambura, and S. Herath, "Link budget analysis for backscatter-based passive IoT," *IEEE Access*, vol. 10, pp. 128 890–128 922, Dec. 2022.
- [4] F. Rezaei, D. Galappaththige, C. Tellambura, and S. Herath, "Coding techniques for backscatter communications - A contemporary survey," *IEEE Commun. Surveys Tuts.*, pp. 1020–1058, 2th Quart. 2023.
- [5] F. Rezaei, C. Tellambura, and S. Herath, "Large-scale wireless-powered networks with backscatter communications—A comprehensive survey," *IEEE open j. Commun. Soc.*, vol. 1, pp. 1100–1130, July 2020.
- [6] C. Song *et al.*, "Advances in wirelessly powered backscatter communications: From antenna/RF circuitry design to printed flexible electronics," *Proc. IEEE*, vol. 110, no. 1, pp. 171–192, Jan. 2022.
- [7] "3GPP TSG RAN Meeting –94e, Study proposal on Passive IoT, 8A.1 (from RP-213368)," Dec. 2021. Available Online: <https://www.3gpp.org/DynaReport/TDocExMtg--RP-94-e--60214.htm>.
- [8] "3GPP TSG RAN –97e3, Study on ambient IoT , 9.1 (from RP-222685)," Sep. 2022. Available Online: <https://portal.3gpp.org/ngppapp/TdocList.aspx?meetingId=60043>.
- [9] R. Long, Y.-C. Liang, H. Guo, G. Yang, and R. Zhang, "Symbiotic radio: A new communication paradigm for passive internet of things," *IEEE Internet Things J.*, vol. 7, no. 2, pp. 1350–1363, 2020.
- [10] X. Lu, N. Cong Luong, D. T. Hoang, D. Niyato, Y. Xiao, and P. Wang, "Secure wirelessly powered networks at the physical layer: Challenges, countermeasures, and road ahead," *Proc. IEEE*, vol. 110, no. 1, pp. 193–209, Jan. 2022.
- [11] H. Kim, *Wireless Communications Systems Design*. Wiley, 2015. [Online]. Available: <https://books.google.ca/books?id=z0lxBwAAQBAJ>
- [12] M. K. Ozdemir and H. Arslan, "Channel estimation for wireless OFDM systems," *IEEE Commun. Surveys Tuts.*, vol. 9, no. 2, pp. 18–48, 2nd Quart. 2007.
- [13] B. Hassibi and B. Hochwald, "How much training is needed in multiple-antenna wireless links?" *IEEE Trans. Inf. Theory*, vol. 49, no. 4, pp. 951–963, Apr. 2003.
- [14] E. Björnson, E. G. Larsson, and M. Debbah, "Massive MIMO for maximal spectral efficiency: How many users and pilots should be allocated?" *IEEE Trans. Wireless Commun.*, vol. 15, no. 2, pp. 1293–1308, Feb. 2016.
- [15] Qualcomm, "Setting off the 5G advanced evolution," Jan. 2022. Available Online: <https://www.qualcomm.com/news/onq/2021/12/10/setting-5g-advanced-evolution>
- [16] S. Ma, G. Wang, R. Fan, and C. Tellambura, "Blind channel estimation for ambient backscatter communication systems," *IEEE Commun. Lett.*, vol. 22, no. 6, pp. 1296–1299, June 2018.
- [17] S. Abdallah, A. I. Salameh, and M. Saad, "Joint channel, carrier frequency offset and IQ imbalance estimation in ambient backscatter communication systems," *IEEE Commun. Lett.*, vol. 25, no. 7, pp. 2250–2254, July 2021.
- [18] W. Zhao, G. Wang, S. Atapattu, and B. Ai, "Blind channel estimation in ambient backscatter communication systems with multiple-antenna reader," in *IEEE/CIC Int. Conf. Commun. China (ICCC)*, Aug. 2018, pp. 320–324.
- [19] W. Zhao, G. Wang, S. Atapattu, R. He, and Y.-C. Liang, "Channel estimation for ambient backscatter communication systems with massive-antenna reader," *IEEE Trans. Veh. Technol.*, vol. 68, no. 8, pp. 8254–8258, Aug. 2019.
- [20] X. Liu, C. Liu, Y. Li, B. Vucetic, and D. W. K. Ng, "Deep residual learning-assisted channel estimation in ambient backscatter communications," *IEEE Wireless Commun. Lett.*, vol. 10, no. 2, pp. 339–343, 2021.
- [21] Y. Zhu, G. Wang, H. Tang, R. He, and Y. Zou, "Channel estimation for ambient backscatter systems over frequency-selective channels," in *IEEE/CIC Int. Conf. Commun. in China (ICCC)*, 2018, pp. 384–388.
- [22] H. Zheng, Z. Yang, G. Wang, R. He, and B. Ai, "Channel estimation for ambient backscatter communications with large intelligent surface," in *11th Int. Conf. on Wireless Commun. and Signal Processing (WCSP)*, 2019, pp. 1–5.
- [23] S. Ma, Y. Zhu, G. Wang, and R. He, "Machine learning aided channel estimation for ambient backscatter communication systems," in *IEEE Int. Conf. Commun. Syst. (ICCS)*, Dec. 2018, pp. 67–71.
- [24] S. Abdallah, Z. Verboven, M. Saad, and M. A. Albreem, "Channel estimation for full-duplex multi-antenna ambient backscatter communication systems," *IEEE Trans. Commun.*, pp. 1–1, Mar. 2023.
- [25] Z. Wang, H. Xu, L. Zhao, X. Chen, and A. Zhou, "Deep learning for joint pilot design and channel estimation in symbiotic radio communications," *IEEE Wireless Commun. Lett.*, vol. 11, no. 10, pp. 2056–2060, Oct. 2022.
- [26] D. Mishra and E. G. Larsson, "Optimal channel estimation for reciprocity-based backscattering with a full-duplex MIMO reader," *IEEE Trans. Signal Process.*, vol. 67, no. 6, pp. 1662–1677, Mar. 2019.
- [27] M. Yerzhanova and Y. H. Kim, "Channel estimation via model and learning for monostatic multi-antenna backscatter communication," *IEEE Access*, vol. 9, pp. 165 341–165 350, Dec. 2021.
- [28] D. Darsena, G. Gelli, and F. Verde, "Joint channel estimation, interference cancellation, and data detection for ambient backscatter communications," in *IEEE 19th Int. Workshop on Signal Processing Advances in Wireless Commun. (SPAWC)*, 2018, pp. 1–5.
- [29] Z. Dai, R. Li, J. Xu, Y. Zeng, and S. Jin, "Rate-region characterization and channel estimation for cell-free symbiotic radio communications," *IEEE Trans. Commun.*, vol. 71, no. 2, pp. 674–687, Feb. 2023.
- [30] L. Wei, C. Huang, G. C. Alexandropoulos, C. Yuen, Z. Zhang, and M. Debbah, "Channel estimation for RIS-empowered multi-user MISO wireless communications," *IEEE Trans. Commun.*, vol. 69, no. 6, pp. 4144–4157, Jun. 2021.
- [31] W. Zhao, G. Wang, S. Atapattu, T. A. Tsiftsis, and X. Ma, "Performance analysis of large intelligent surface aided backscatter communication systems," *IEEE Wireless Commun. Lett.*, vol. 9, no. 7, pp. 962–966, Feb. 2020.
- [32] L. Yang, Y. Yang, M. O. Hasna, and M.-S. Alouini, "Coverage, probability of SNR gain, and DOR analysis of RIS-aided communication systems," *IEEE Commun. Lett.*, vol. 9, no. 8, pp. 1268–1272, Aug. 2020.
- [33] R. Zhang and C. K. Ho, "MIMO broadcasting for simultaneous wireless information and power transfer," *IEEE Trans. Wireless Commun.*, vol. 12, no. 5, pp. 1989–2001, May 2013.
- [34] P. Lu, K. Huang, C. Song, Y. Ding, and G. Goussetis, "Optimal power splitting of wireless information and power transmission using a novel dual-channel rectenna," *IEEE Trans. Antennas Propag.*, vol. 70, no. 3, pp. 1846–1856, Mar. 2022.
- [35] D. Galappaththige, F. Rezaei, C. Tellambura, and S. Herath, "RIS-empowered ambient backscatter communication systems," *IEEE Wireless Commun. Lett.*, vol. 12, no. 1, pp. 173–177, Jan. 2023.
- [36] S. M. Kay, *Fundamentals of statistical signal processing: estimation theory*. Prentice-Hall, Inc., 1993.
- [37] K. J. Horadam, *Hadamard matrices and their applications*. Princeton university press, Jan. 2012.
- [38] J. G. Andrews, "A primer on zadoff chu sequences," *arXiv preprint arXiv:2211.05702*, 2022.
- [39] M. Biguesh and A. B. Gershman, "Training-based MIMO channel estimation: A study of estimator tradeoffs and optimal training signals," *IEEE Trans. Signal Process.*, vol. 54, no. 3, pp. 884–893, 2006.
- [40] J. Seberry, B. JWysocski, and T. AWysocski, "On some applications of hadamard matrices," *Metrika*, vol. 62, pp. 221–239, 2005.
- [41] K. R. Rao and P. C. Yip, *The transform and data compression handbook*. CRC press, Oct. 2018.
- [42] M. Biguesh and A. B. Gershman, "Downlink channel estimation in cellular systems with antenna arrays at base stations using channel probing with feedback," *EURASIP J Adv. Signal Process.*, vol. 2004, pp. 1–10, Dec. 2004.
- [43] F. Rezaei, C. Tellambura, A. A. Tadaion, and A. R. Heidarpour, "Rate analysis of cell-free massive MIMO-NOMA with three linear precoders," *IEEE Trans. Commun.*, vol. 68, no. 6, pp. 3480–3494, June 2020.
- [44] D. Galappaththige and G. A. A. Baduge, "Exploiting underlay spectrum sharing in cell-free massive MIMO systems," *IEEE Trans. Commun.*, vol. 69, no. 11, pp. 7470–7488, Nov. 2021.

- [45] T. Marzetta, E. Larsson, H. Yang, and H. Ngo, *Fundamentals of Massive MIMO*. Cambridge University Press, 2016. [Online]. Available: <https://books.google.ca/books?id=Be08DQAAQBAJ>
- [46] “3GPP TR 36.814, further advancements for E-UTRA physical layer aspects, V.9.0.0 Rel. 9,” Mar. 2010. Available Online: <https://portal.3gpp.org/desktopmodules/Specifications/SpecificationDetails.aspx?specificationId=2493>.
- [47] T. Schenk, *RF Imperfections in High-Rate Wireless Systems: Impact and Digital Compensation*, 1st ed. Springer Publishing Company, Incorporated, 2008.
- [48] X. Li, M. Zhao, Y. Liu, L. Li, Z. Ding, and A. Nallanathan, “Secrecy analysis of ambient backscatter NOMA systems under I/Q imbalance,” *IEEE Trans. Veh. Technol.*, vol. 69, no. 10, pp. 12 286–12 290, 2020.
- [49] X. Li *et al.*, “Hardware impaired ambient backscatter NOMA systems: Reliability and security,” *IEEE Trans. Commun.*, vol. 69, no. 4, pp. 2723–2736, 2021.
- [50] C. Liu, Z. Wei, D. W. K. Ng, J. Yuan, and Y.-C. Liang, “Deep transfer learning for signal detection in ambient backscatter communications,” *IEEE Trans. Wireless Commun.*, vol. 20, no. 3, pp. 1624–1638, Mar. 2021.